Review

Advances in engineering near-infrared luminescent materials

Christopher T. Jackson,[1] Sanghwa Jeong,[1] Gabriel F. Dorlhiac,[2] and Markita P. Landry[1,3,4,5,*]

Near-infrared (NIR) luminescent materials have emerged as a growing field of interest, particularly for imaging and optics applications in biology, chemistry, and physics. However, the development of materials for this and other use cases has been hindered by a range of issues that prevents their widespread use beyond benchtop research. This review explores emerging trends in some of the most promising NIR materials and their applications. In particular, we focus on how a more comprehensive understanding of intrinsic NIR material properties might allow researchers to better leverage these traits for innovative and robust applications in biological and physical sciences.

INTRODUCTION

The search for new luminescent materials that emit in the NIR region, from ~700 to 2500 nm, has rapidly expanded in recent years. In contrast to their counterparts that emit at shorter wavelengths, mostly in the visible spectrum, NIR emissive materials possess a number of unique advantages. NIR light can penetrate biological tissues with minimum interference due to reduced absorption and scattering by tissues, such as skin and blood, in this wavelength range (Smith et al., 2009). Further, because water absorbs in the visible spectrum, NIR emissive materials enjoy enhanced bioimaging capabilities (Hong et al., 2017). In principle, the energy involved with the generation and decay of excited species in NIR emission is much smaller than for UV or visible emission (Zampetti et al., 2019), which limits the number of side reactions that may take place, increasing the expected stability of NIR materials and devices. Materials that absorb and emit in the NIR region can be used for inexpensive laser diode excitation, as photodetectors, and as optical sources themselves. Collectively, these properties allow for a diverse range of potential applications, including biological imaging, therapy, communications, and display technologies.

However, there remain a number of outstanding problems that hinder the applicability of these NIR materials outside of laboratory conditions, particularly *in vivo*. Typically, these materials have suffered from poor stability, low quantum yield, and limited tunability; a brief comparison of these challenges, alongside other material properties across different NIR materials, is provided in Table 1. Solutions to these problems are necessary for the deployment of NIR-emitting materials in commercial applications and for broader in-laboratory use and therefore this remains an area of ongoing research. As these tools are used by a growing and diverse community of researchers, it is critical to examine the underlying chemistry and physics that enable their successful development and deployment. A better understanding of these intrinsic material properties, particularly across different types of NIR-emitting materials, will ultimately drive research toward new applications.

In this review, we explore the photophysics of NIR emission in organic dyes, carbon nanomaterials, inorganic nanoparticles, and proteins, with a focus on how NIR emitters can be tailored to overcome new challenges faced by the NIR research community. We further examine the opportunities to apply NIR-emitting materials in light sources and detection to enable the next generation of optoelectronic devices.

ORGANIC DYES

Organic dyes that are optically active in the NIR region of the electromagnetic spectrum have a longstanding history of use in imaging, targeting, and treatment in biological systems. Upon excitation by an energy source, electrons transition from the highest occupied molecular orbital (HOMO) to the lowest unoccupied molecular orbital (LUMO). By tuning the length of the unsaturated carbon chains and the makeup of chemical groups that act as electron sinks within the dye, electrons can be delocalized to tune the light that is emitted following this excitation (Figure 1F). Therefore, to achieve emission in the NIR, it is necessary to develop dyes with intramolecular π-conjugated systems and substituent electronic effects (Gong et al.,

[1]Department of Chemical and Biomolecular Engineering, University of California, Berkeley, CA, USA

[2]Biophysics Graduate Group, University of California, Berkeley, CA, USA

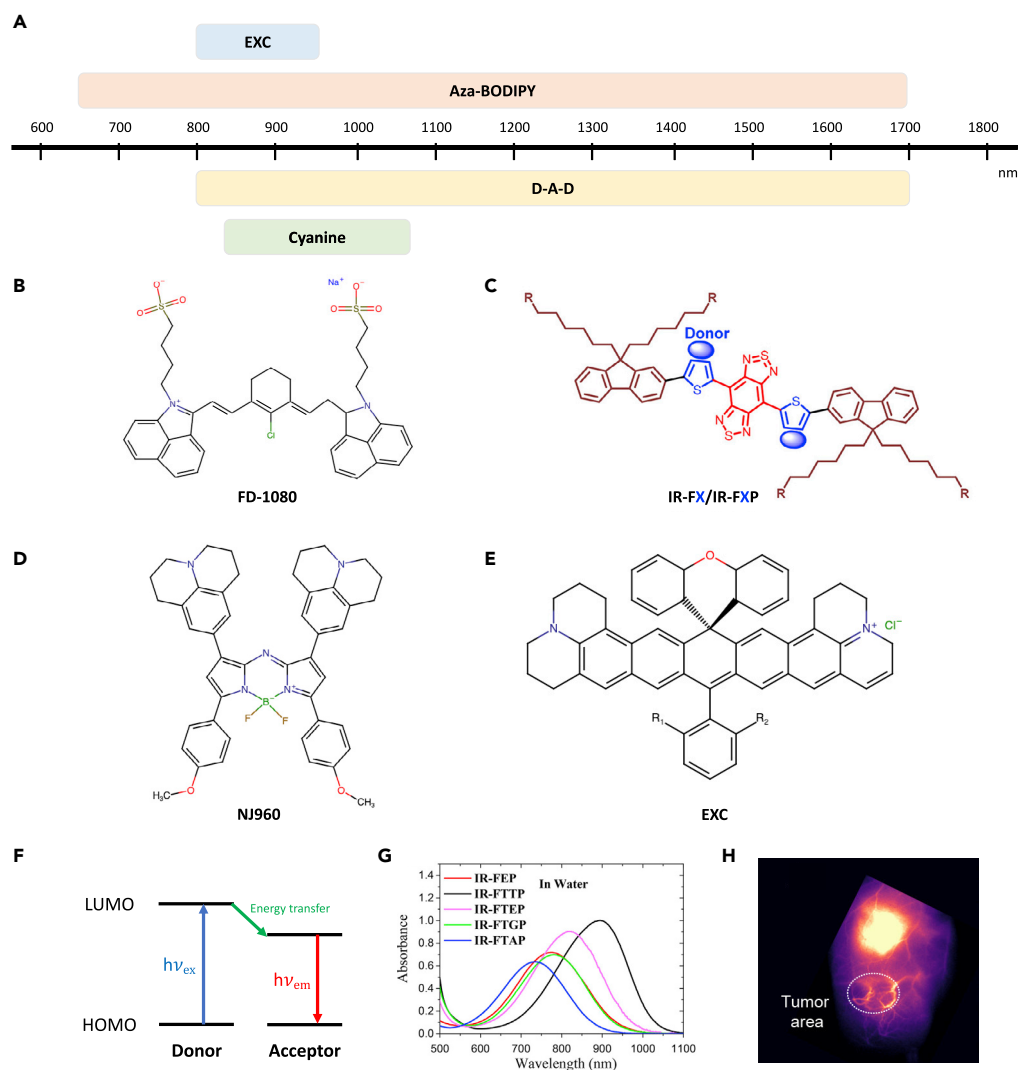[3]Innovative Genomics Institute (IGI), Berkeley, CA, USA

[4]California Institute for Quantitative Biosciences, QB3, University of California, Berkeley, CA, USA

[5]Chan-Zuckerberg Biohub, San Francisco, CA, USA

*Correspondence:
landry@berkeley.edu

https://doi.org/10.1016/j.isci.2021.102156

Figure 1. NIR-emitting organic dyes

(A) Schematic illustrating the reported tunable emission wavelength range of various classes of organic dyes.

(B) Cyanine dye.

(C) D-A-D dye with shielding units.

(D) Aza-BODIPY dye.

(E) EXC dye.

(F) Modulation of the HOMO-LUMO gap via tuning of molecular structure.

(G) Absorbance spectra of PEGylated D-A-D fluorophores in aqueous solution.

(H) NIR-II image of a mice tumor after intravenous injection of an aza-BODIPY based dye. Panels c and g are reproduced from (Yang et al., 2018); Copyright 2016, American Chemical Society. Panel h is reproduced from (Godard et al., 2020); Copyright 2020, American Chemical Society.

2016). High energy absorption and emission (300–600 nm) can be attributed to π-π* and n-π* transitions of conjugated structures, whereas lower energies (600–1400 nm) are typically due to intramolecular charge transfer between peripheral donors (Qian et al., 2012). Small molecule organic dyes are particularly useful due to their well-defined and tunable structures; here we will focus on four categories: cyanine, donor-acceptor-donor (D-A-D), aza-BODIPY, and EXC dyes (Figure 1A).

Cyanine

Cyanine-based dyes have been used extensively in bioimaging, with indocyanine green (ICG) being an NIR dye with emission at ~830 nm clinically approved by the FDA since 1959; however, ICG suffers from low quantum

yield (QY) in aqueous solution, poor stability, rapid clearance, and cytotoxicity (Carr et al., 2018; Escobedo et al., 2010). To address these issues, while drawing from the ICG structure that affords a high absorption coefficient, recent cyanine dyes use a polymethine scaffold, consisting of heterocycles linked by a methine chain (Cosco et al., 2017). Traditional cyanine dyes have spanned the visible and NIR-I region by increasing the length of the methine chain. Cosco et al. demonstrated that by using a 7-dimethylamino flavylium heterocycle, the emission of these cyanines can be controllably red-shifted even further, to 1064 nm (Cosco et al., 2017, 2020). Other work has similarly drawn from the ICG structure to develop polymethine dyes with absorption and emission in the NIR-II region. Whereas ICG absorbs and emits in the NIR-I region, substitution of the nitrogens in the ICG structure for oxygens leads to NIR-I excitation and NIR-II emission; substitution with sulfurs leads to both excitation and emission in the NIR-II region (Ding et al., 2019).

To address issues of low QY, a rigid molecular structure can be adopted to minimize nonradiative decay. Li et al. demonstrated that modifying the ICG structure with a conjugated methine chain and cyclohexene and sulfonic groups could enhance its water solubility and stability. This yielded a dye (FD-1080) with a QY of 0.31% (increased to 5.94% in fetal bovine serum) that can be excited at 1064 nm and emitted at 1080 nm (Figure 1B) (Li et al., 2018a). This excitation in the NIR-II region allows for deeper penetration depth and higher resolution *in vivo* imaging due to reduced tissue scattering. Dyes adopting this structure have also demonstrated greater chemical stability in aqueous solutions and improved photostability compared with ICG (Lei et al., 2019).

Attempts have been made to extend these dyes to excitation and emissions at longer wavelengths by lengthening the polymethine chain. Although this approach does increase the wavelength of emission, it also typically causes significant solvatochromic quenching in polar solvents, limiting their use in bioimaging applications (Wang et al., 2019). Therefore, more work is needed to generate red-shifted dyes with high QYs in polar environments through methods such as enhancing the donor strength of the molecule's heterocycles, branching the polymethine chain, or engineering the charge of the π-system.

D-A-D

Donor-acceptor-donor (D-A-D) type small molecule fluorescent dyes offer another mechanism to tune the band gap of π-conjugated semiconductors and achieve NIR optical properties. Antaris et al. reported the first use of this structure to synthesize CH1055, a water soluble PEGylated NIR-II fluorophore with a molecular mass of 8.9 kDa and emission at 1055 nm (Antaris et al., 2016). However, this reduced band gap often leads to increased interactions between the dye's conjugated backbone and other molecules, causing aggregation and quenching fluorescence QY. To address this problem, Yang et al. added a dialkyl fluorene as the shielding unit to synthesize IR-FEP, a pegylated shielding unit-donor-acceptor-donor-shielding unit (S-D-A-D-S) structure with BBTD as the acceptor and EDOT (3,4-ethylenedioxythiophene) as the donor (Figure 1C) (Yang et al., 2017). These additions enabled tunable NIR absorbance (Figure 1G) and increased QY to 2% in aqueous solution, from the previous 0.4% QY of the shielding unit-free counterpart.

Adopting this S-D-A-D-S structure, subsequent work has explored donor engineering to enhance fluorescence performance (Yang et al., 2018). By using octylthiophene as the first donor, the bulky, hydrophobic group causes a larger distortion of the conjugated backbone and fewer interactions with surrounding water molecules. At the same time, thiophene is used as the second donor, increasing the conjugation length and red-shifting the fluorescence emission to 1048 nm with a QY of 5.3% in aqueous solution.

To broaden NIR applications, particularly for multiplexed imaging, it is necessary to increase the number of fluorescent channels available with non-overlapping emission spectra. Zhu et al. have developed a clickable organic fluorophore and a carbon nanotube fluorescent agent conjugated to molecularly specific proteins or antibodies that can be purified through density gradient ultracentrifugation separations (Zhu et al., 2017). This approach enabled multicolor biological imaging in the 800 to 1700 nm NIR window with a QY of 1.9% in aqueous solution. Future work, particularly for multiplexed imaging, must focus on constructing molecular dyes with higher QYs, narrow emission wavelengths, and large Stokes shifts.

aza-BODIPY

Aza-dipyrromethene boron difluoride (aza-BODIPY) dyes represent another class of NIR emitters with unique optical properties and sufficient water solubility for *in vivo* imaging applications. Although commercially available aza-BODIPY dyes emit in the NIR-I region (650–1000 nm), Bai et al. have reported molecular

engineering techniques using aza-BODIPY as an acceptor (A) and strong electron-donating groups as donors (D) to create a strong D to A intramolecular charge transfer effect that red-shifts their emission to the NIR-II window (1000–1700 nm) (Figure 1D) (Bai et al., 2019). Parallel work by Godard et al. has reported a strategy to introduce ammonium atoms onto the central boron atom of aza-BODIPY, creating a water-soluble NIR-II fluorophore that was used for *in vitro* and *in vivo* tumor imaging in mice (Figure 1H) (Godard et al., 2020). These BODIPY-based dyes are also significantly easier to synthesize than cyanine and D-A-D based structures, presenting the possibility of further design to improve their quantum yield.

EXC

EXC dyes, a new family of NIR fluorescent dyes with absorption and emission in the NIR region (abs. 880 nm, em. 915 nm), are able to mitigate some of the challenges that other small molecular dyes have typically faced (Lei et al., 2017). EXC dyes are based on a bisbenzo-C-rhodamine unit modified with a diphenyl ether moiety through spiro linkage. This bulky diphenyl ether group sterically hinders the rotational freedom of the molecule, preventing undesirable non-radiative quenching. Lei et al. have also demonstrated post-synthetic modifications attaching different chemical handles or functional groups that allow tuning of the quantum yield above 10% in organic solvents and 1.4% in aqueous solution (Figure 1E) (Lei et al., 2017).

CARBON NANOMATERIALS

Given the challenges associated with fluorescent organic dyes, in recent years a growing interest in alternative luminescent materials has emerged. In particular, carbon-based nanomaterials demonstrate a resistance to photobleaching, enabling their use in a wider variety of imaging techniques over long timescales, while sometimes offering additional improvements in luminescence brightness (Algar, 2020). To improve the applicability of carbon-based nanomaterials in bioimaging, techniques have been developed to coat carbon nanomaterials with polymers such as polyethylene glycol to produce materials that are both bright and biocompatible (Welsher et al., 2009). Here we highlight single-walled carbon nanotubes (SWNTs) and carbon dots as two promising candidates for highly stable and tunable NIR-emitting materials.

Single-walled carbon nanotubes

SWNTs are quasi-one dimensional structures that can be conceptualized as the rolling of a graphene sheet (Figure 2A). Their unique optical properties, particularly their NIR emission (∼700–1800 nm), arise from Van Hove singularities in their electronic density of states that can be tailored by the tuning of the nanotube's chiral angle (Figure 2B) and electronic contributions of molecules bound to their surface (Pan et al., 2017; Bachilo et al., 2002). The absorption peak wavelength of a SWNT varies with the mean tube diameter, whereas the absorption spectral bandwidth is dependent on the nanotube diameter distribution (Yamashita, 2019). SWNTs offer unique advantages for imaging, including no blinking or photobleaching and further chemical tunability through adsorption of ligands via π-π stacking interactions. However, recent research still seeks to understand how biological environments impact SWNT physicochemical properties to reach the levels of biocompatibility achieved by NIR-emitting organic dyes and proteins (Pan et al., 2017; Pinals et al., 2020).

Chirality-dependent emission

SWNT chirality gives rise to chirality-specific physical and optical properties, providing a distinct spectroscopic signature for each chirality (Figure 2C) (Pan et al., 2017). Generally, chirality-pure SWNT samples have singular excitation and emission maxima, enabling single-chirality SWNTs to be used as monochromatic fluorescent reporters for infrared imaging. (6,5) chirality-pure SWNTs are particularly desirable for bioimaging applications due to their increased brightness compared with mixed-chirality SWNTs and their relative ease of purification compared with other chiralities (Antaris et al., 2013; Danné et al., 2018; Roxbury et al., 2015). However, purification of individual SWNT chiralities from the multi-chirality mixtures resulting from their synthesis can be challenging. Recent approaches to SWNT chirality purification have identified techniques, referred to as a corona phase exchange purification (CPEP) using polyfluorene polymers to enrich certain SWNT chiralities, which can then be redispersed in desired organic phase (Nißler et al., 2019). The authors demonstrated that these chirality-pure SWNTS could be further dispersed in water by exchanging the surface functionalizations to aqueous soluble surfactants or polymers, thus enabling their broader use in applications such as bioimaging.
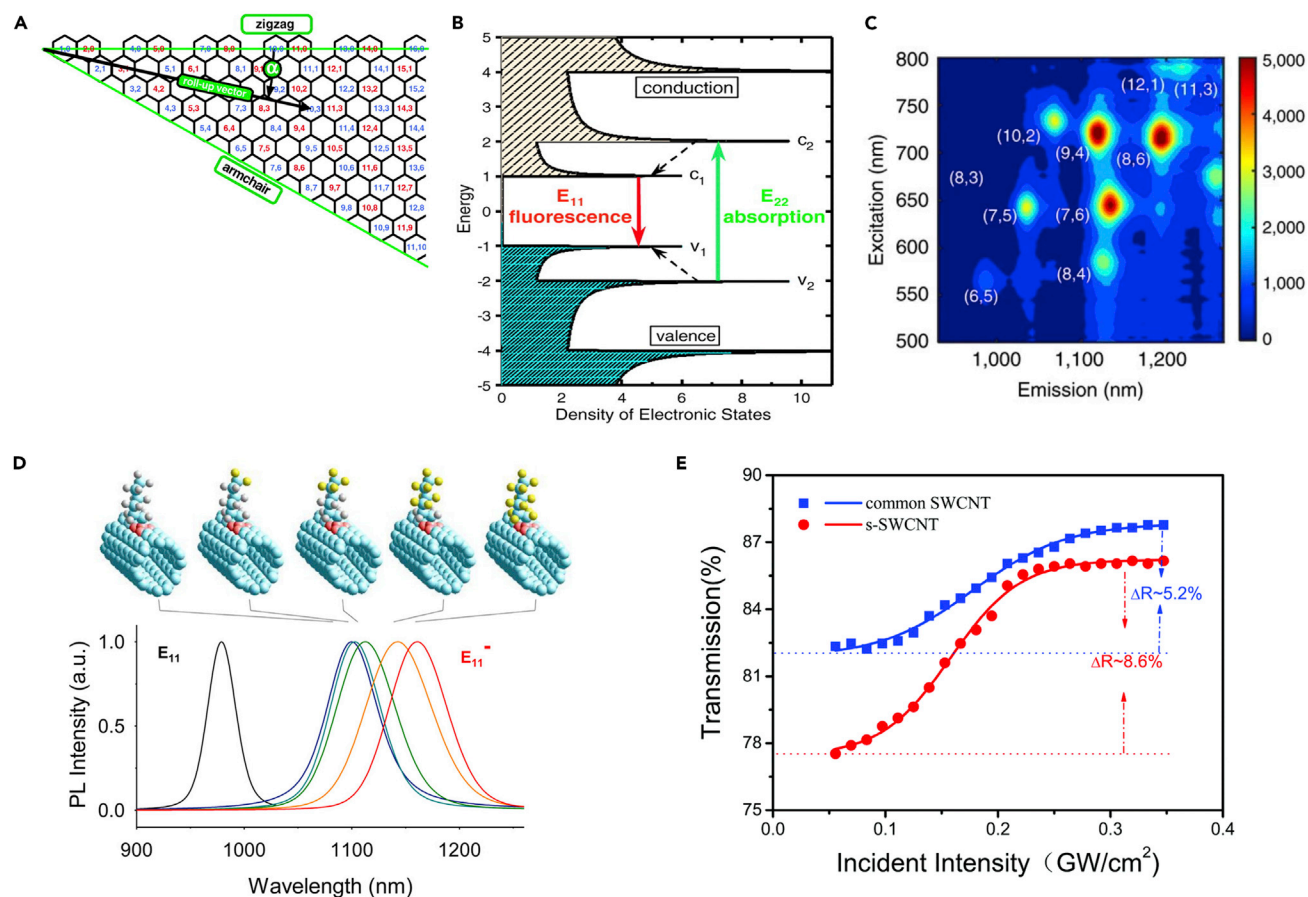
Figure 2. Single-walled carbon nanotubes (SWNTs)

(A) Schematic showing the formation of different chirality carbon nanotubes obtained by rolling a graphene sheet from different lattice points.

(B) Schematic electronic density of states for a single carbon nanotube, where E_{11} fluorescence can be modulated via the tuning of the nanotube's chiral angle.

(C) Excitation-emission profile of a mixed chirality DPPE-PEG(500)-wrapped SWNT solution.

(D) Tunable photoluminescence (PL) spectra of (6,5)-SWCNTs functionalized with six-carbon alkyl chains with increasing numbers of fluorine substituents.

(E) Nonlinear transmission versus the incident intensity for samples of mixed and pure-semiconducting SWNTs. Panels A and B are reproduced from (Bachilo et al., 2002); Copyright 2002, The American Association for the Advancement of Science. Panel C is reproduced with permission from (Bisker et al., 2016); Copyright 2016, Springer Nature. Panel D is reproduced from (Kwon et al., 2016); Copyright 2016, American Chemical Society. Panel E is reproduced from (Shi et al., 2019); Copyright 2019, Royal Society of Chemistry.

Given the strong dependence of SWNTs on their local dielectric environment, multiple studies have explored the effect of SWNT chirality and SWNT fluorescence on their interactions with biomolecules, particularly DNA, and subsequent changes in fluorescence. Early work by Heller et al. demonstrated the ability to transduce the conformational rearrangement of a bound DNA molecule on the SWNT surface while at the same time modulating the SWNT's dielectric environment and decreasing NIR emission by up to 15 meV. Salem et al. found that different single-stranded DNA sequences, particularly $(TAT)_4$ and $(ATTT)_3$, formed DNA-SWNT hybrids with chirality-dependent fluorescence responses to various analytes (Salem et al., 2016). Similar studies have found that for $(GT)_6$, a common DNA sequence used to suspend SWNTs for optical sensing, the stability of constructs depends on molecular interactions between the DNA sequence and specific SWNT chirality, not DNA sequence length or chirality (Jena et al., 2017). This chirality dependence has been applied to SWNT sensors for dopamine using NIR-II excitation and fluorescence with a quantum efficiency of 0.23%. These sensors show chirality-dependent responses for dopamine with fluorescent turn-on responses between 20% and 350% (Bonis-O'Donnell et al., 2017).

Defect-oriented emission

SWNT defects, traditionally viewed as detriments to NIR optical applications, have recently gained new attention as an exciting field of research for fluorescence tunability (Brozena et al., 2019). Although most defect engineering is limited by chemistries only possible in aqueous solution, recent progress has been made toward new methods using organic solvents. One of the first reports showing chemical control of defect quantum states in SWNTs demonstrated emission from aryldiazonium defects brighter than that of the pristine SWNTs. This emission is tunable by as much as 254 meV by attachment of electron-withdrawing substituents; QY increased exponentially as a function of the shifted emission energy and reached up to 16%, one of the brightest reports of SWNTs in water (Piao et al., 2013).

More recently, SWNT defects have been harnessed to tailor excitonic behavior through molecular engineering of covalently attached surface functional groups. Kwon et al. demonstrated the use of alkyl and aryl defects to tune fluorescence through their inductive electronic effect. Although the quantum defects trap excitons at a localized potential well, the SWNT serves as an antenna to harvest light and channel excitons to the defect site, where excitons recombine and give off NIR emission dependent on the tailored functional group (Figure 2D) (Kwon et al., 2016). These arylated SWNTs can also be tailored for use as pH sensors; the authors demonstrated that switching between protonated and deprotonated states of an attached amine modified its defect state, producing energy shifts that were sensitive to pH changes as small as 0.2 pH units over a pH range of 4.5–8.5 (Kwon et al., 2015). As subsequent studies showed, excitons trapped at defect sites are not subject to diffusion-limited contact quenching, allowing for radiative relaxation and red-shifted emission. By tuning the defect density, Berger et al. reported enhanced QY up to 4% (Berger et al., 2019). Recent research has also used quantum defects for modular anchors for both the attachment of nanobodies (such as peptides and proteins) and the synthesis of peptides directly on the SWNT surface, enabling further tuning of their photophysical properties (Mann et al., 2020).

Nonlinear optical properties

The nonlinear optical properties of SWNTs include saturable absorption, two-photon absorption, modulation depth, and optical limitations of decreased transmittance under high-intensity illumination (Shi et al., 2019). These properties can be traced to the basis of SWNT structure, the cylindrical wrapping from a graphene sheet, transitioning from a 2D topology to a quasi-1D topological structure. This reduced dimensionality leads to a quantum confinement of the π-electron wavefunction in the radial and circumferential directions, contributing to a delocalized π-electron system confined by a quasi-1D structure (Figure 2E) (Shi et al., 2019).

Using Z-scan and pump-probe spectroscopy across 600–2400 nm, Xu et al. demonstrated the mapping of nonlinear absorption properties across a broad spectral range. Their spectral results indicate that saturable absorption occurs across the visible and near-IR range, with a cutoff within the semiconducting S_{11} band that indicates the role of photoinduced effects in addition to physical effects such as Pauli blocking (Xu et al., 2016a, 2016b). Other recent studies suggest that nonlinear photoemission is a result of optical-field-driven electron tunneling from the valence band; therefore, emission nonlinearity can be tuned by engineering the SWNT band structure through techniques such as controlling the SWNT chirality and doping level (Li et al., 2019a).

Carbon dots

Carbon dots are quasi-spherical fluorescent nanoparticles consisting of sp^2 carbon atoms and sp^3 carbon atoms at edge planes with dimensions less than 10 nm in diameter. Graphene quantum dots are a subset of carbon dots with higher crystallinity and fewer defects (Li et al., 2019b). Fluorescent carbon dots usually emit in the UV and visible spectrum; however, recent advances in their fabrication have enabled fluorescent carbon dots emitting at over 1000 nm. Tang et al. demonstrated the microwave-assisted hydrothermal synthesis of nitrogen-doped graphene quantum dots with broadband photoluminescence from deep UV to NIR wavelength upon excitation with 808 nm light (Tang et al., 2014). The unusual NIR emission from graphene quantum dots likely originates from the conjugated electrons in their layered structure. More recently, Li et al. reported the fabrication of NIR-emitting carbon dots from watermelon juice via a hydrothermal method. These carbon dots exhibited NIR emission from 900 to 1200 nm with a decent quantum yield of 0.4% (Li et al., 2019c). Similar to previous reports, these carbon dots had a quasi-spherical structure
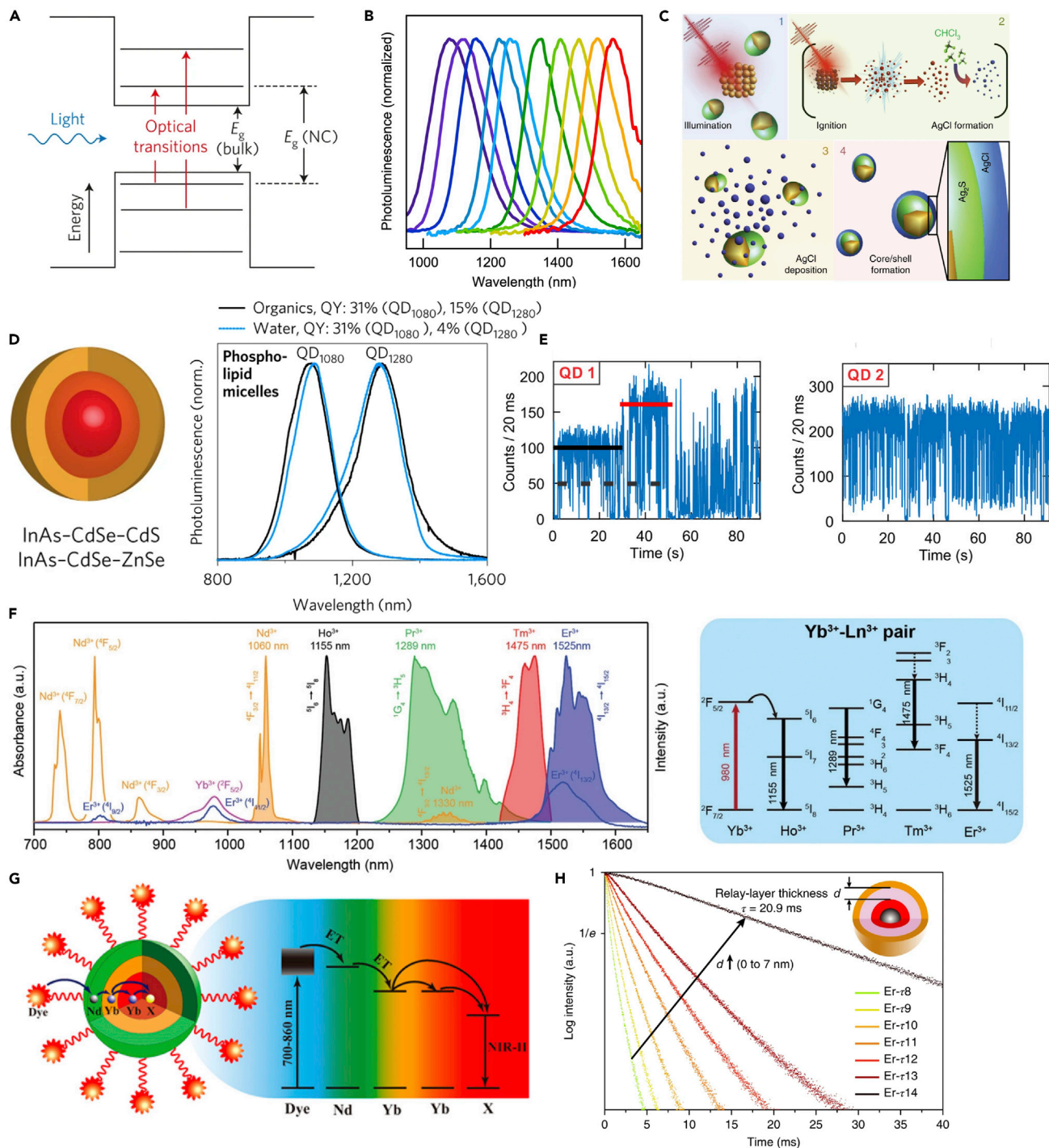
Figure 3. NIR luminescent inorganic nanoparticles

(A) Energy diagram of QDs with tunable band gap.

(B) Tunable NIR PL wavelength of PbS QDs by size control.

(C) Schematic illustration of the transformation from Ag_2S nanodots to Ag_2S superdot by ultrafast laser pulse.

(D) Highly bright InAs-based QD in aqueous phase.

(E) Two characteristic blinking behaviors of QDs.

(F) Absorption and downconverted NIR emission spectrum of various lanthanide ions and proposed energy transfer mechanism for NIR emission in Yb^{3+} and Ln^{3+} paired systems.

(G) Absorption-enhanced NIR-emitting La NPs by antenna effect from surface-conjugated dyes.

Figure 3. *Continued*
(H) High tunable NIR radiative lifetime of La NPs by controlling the relay-layer thickness between sensitizer and activators. Panel B is reproduced with permission from (Weidman et al., 2014); Copyright 2014, American Chemical Society. Panel c is reproduced with permission from (Santos et al., 2020); Copyright 2020, Springer Nature. Panel D is reproduced with permission from (Bruns et al., 2017); Copyright 2017, Springer Nature. Panel E is reproduced with permission from (Yuan et al., 2018); Copyright 2018, American Chemical Society. Panel F is reproduced with permission from (Fan and Zhang, 2019); Copyright 2019, Wiley-VCH GmbH. Panel G is reproduced with permission from (Shao et al., 2016); Copyright 2012, Springer Nature. Panel H is reproduced with permission from (Fan et al., 2018); Copyright 2018, Springer Nature.

with diameters less than 10 nm and consisted of oxygen- and nitrogen-related functional groups (Tang et al., 2014).

INORGANIC NANOPARTICLES

Compared with their organic counterparts, inorganic nanoparticles can benefit from a wide variety of useful properties, including non-toxicity, hydrophilicity, biocompatibility, and high stability. In recent years, quantum dots and lanthanide nanoparticles have emerged as two particularly exciting candidates for use as tunable and highly luminescent NIR emitters.

Semiconductor quantum dots

The optical properties of semiconductors are determined by excitons (excited hole-electron pairs) that have an intrinsic Bohr radius where the kinetic energy and Coulombic potential are ideally balanced. When the dimensions of a semiconductor are similar to or smaller than its Bohr radius, the excessive Coulombic potential results in a quantum confinement effect. This principle forms the basis of quantum dots (QDs). In the quantum confinement regime, energy levels are quantized to discrete values and the band gap of a QD depends on its size; specifically, the band gap increases when the size decreases (Figure 3A). QDs usually range in size from 2 to 10 nm and consist of 100 to 100,000 atoms in a single particle. The band gap energy and emission wavelength of QDs can be easily tuned by adjusting their size, where the broad absorption profile of the QD enables wavelength-independent excitation of QDs. In comparison to other NIR fluorophores, QDs have advantages such as a broad absorption spectrum, high PL QY, large Stokes shift, and excellent band-gap tunability.

Types of NIR-emitting QDs

In the last decade, research on NIR-emitting QDs has focused on metal chalcogenides. QDs composed of lead chalcogenides such as PbS have exhibited decent NIR absorption and emission capabilities in photovoltaic devices. The emission spectra of PbS QDs are extensively tunable in the range of 900–2000 nm by adjusting their size (Figure 3B) (Weidman et al., 2014). The emission wavelength of NIR-emitting QDs can be easily tuned by controlling their size, which enables outstanding multispectral characteristics among current NIR emitters. The high monodispersity and gaussian-like emission spectrum of QDs enables narrow absorption and emission peaks that have half-width at half maximum values in the ranges of 20–40 meV. Due to their extensive study, high-quality synthesis techniques exist that can improve their monodispersity (standard deviation of the QD size distribution ~4%) and brightness (up to 100% QY) (Moreels et al., 2011). The chemical stability of PbS QDs can be improved by using an inorganic protective shell such as a CdS/ZnS multi shell structure, which further increases PL QY by passivating defect states (Jeong et al., 2017). However, medical applications of QDs are limited by concerns about the potential leakage of Pb, a heavy metal ion. Although some researchers report minimal cytotoxicity up to several months in mice, the biocompatibility of Pb-based QDs warrants further investigation (Park et al., 2017).

Ag_2S QDs can enable NIR imaging and are known to have higher biocompatibility due to the absence of heavy metal ions in their composition, lending themselves to various applications ranging from bioimaging probes to NIR-emitting devices (Xu et al., 2016a, 2016b). The emission wavelength of Ag_2S QDs is tunable from 500 to 1200 nm via size control. However, the chemical instability of Ag_2S QDs often results in their structural and optical deterioration under light and redox conditions. Although deterioration might be ameliorated by the fabrication of an inorganic protective shell, this approach has not been fully investigated for Ag_2S QDs. Recently, femto-second laser pulsing of Ag_2S dots prompted the transformation of Ag-Ag_2S heterodimers to highly fluorescent Ag_2S superdots that contain protective AgCl outer shells (Figure 3C) (Santos et al., 2020). This transformation results from the fast dissolution of Ag nanoparticles and subsequent reaction between Ag atoms and Cl atoms from chloroform solvent to passivate the Ag_2S

dots with the AgCl shell. Using ultrafast illumination of 50 fs pulses drastically reduces surface-related non-radiative processes and leads to an increased QD PL QY of up to 10% and a longer fluorescence lifetime in this Ag_2S system.

As the most recently reported composition of NIR QDs, InAs QDs have been introduced as bright and photostable NIR QDs with a tunable emission spectrum (1000–1400 nm). Bright and photostable InAs-based QDs such as InAs/CdSe/CdS core/shell/shell QDs have been synthesized by continuous injection synthesis. The QY of InAs-based QDs have reached 30% in aqueous solution with PL lifetimes of 100 ns, enabling *in vivo* whole body imaging with >50 frames per second and negligible background signal (Figure 3D) (Bruns et al., 2017). Furthermore, InAs-based QDs show high PL QY in aqueous environments relative to other QDs. However, the long-term toxicity of InAs-based QDs needs to be studied further before consideration of their use in humans.

Controlling blinking and quantum yield

Among all NIR fluorescent emitters, including organic dyes, carbon nanomaterials, and lanthanides, QDs have shown the highest QY (up to 100%). The PL lifetime of NIR QDs is usually 10 ns–1 μs, longer than organic dyes and SWNT and shorter than lanthanide-doped nanomaterials (Table 1) (Park et al., 2017). Because QDs have such a high surface-to-volume ratio, the radiative recombination of excitons in QDs (closely tied to QY), is highly dependent on their surface states. To maximize QY, it is necessary to use inorganic and organic protective layers to minimize surface trap sites such as nonstoichiometry and dangling bonds (Zhang et al., 2018).

QDs exhibit a unique blinking behavior, where photoluminescence stochastically fluctuates on a timescale ranging from milliseconds to tens of seconds. The widely accepted explanation for this phenomenon is that a transient charged state is created by illumination, which then promotes non-radiative excitonic relaxation via *Auger* recombination (Efros and Nesbitt, 2016). Although blinking may be neglected in ensemble measurements, the optical measurement of a single QD probe can be detrimental if a stable fluorescence signal is desired. Yuan et al. recently reported experimental evidence that suggests the coexistence of two blinking pathways in a single QD—one due to fluctuations in adsorbate at the crystal surface (BC-blinking) and a second involving both radiative and nonradiative rate-jumps due to charging (Auger-blinking) (Figure 3E) (Yuan et al., 2018). Previous reports suggest that non-blinking QDs can be made by controlled epitaxial inorganic shell growth on the QD core, potentially leading to higher QY and more consistent fluorescence outputs (Javaux et al., 2013).

Photostability

The photostability of NIR QDs has been understudied, especially in comparison to that of visible QDs. It is generally accepted that the photostability of NIR QDs is much higher than that of organic NIR dyes. This increased photostability of QDs is attributed to their controlled inorganic structure and stable organic ligands, which reduces the formation of surface trap sites and prevents particle aggregation via ligand desorption. By using a slow and continuous injection of precursors, Franke et al. synthesized InAs QDs that exhibited less than 10% photobleaching upon >100 mW/cm^2 irradiation and up to two months of photostability (Franke et al., 2016). More recently, Zamberlan et al. reported PbS QDs capped with dihydrolipoic acid–polyethylene glycol ligands, with stable photoluminescence for up to 9 months (Zamberlan et al., 2018).

Lanthanide-doped nanoparticles

Lanthanide-doped nanoparticles (La NPs) usually consist of a host nanomaterial, a sensitizer, and an activator. Host nanomaterials, which provide the template for lanthanide dopants, must be transparent to allow for excitation and emission light to pass through. Various kinds of lanthanide dopant ions have been used as "sensitizers," which absorb excitation light and transfer the harvested energy to the "activator" that in turn emits photoluminescence (e.g. Yb, Er-doped $NaYF_4$).

Conventionally, La NPs have been extensively studied as upconversion PL probes, converting near-infrared irradiation into visible PL. More recently, the downconversion of visible light to NIR by La NPs has emerged as an area of interest in NIR probe development. La NPs exhibit advantageous NIR optical properties compared with other NIR probes including a low level of photobleaching, narrow emission

bandwidth, non-photoblinking, and feasible time-gated lifetime imaging based on their long radiative lifetime.

Tuning the emission of La NPs

Numerous NIR-emitting La NPs have been reported with different host materials and sensitizer/activator ions. A number of transparent inorganic matrices in the visible and NIR window have been used as the host material for NIR-emitting La NPs including $NaYF_4$, $NaCeF_4$, $NaGdF_5$, LaF_3, and Y_2O_3. As sensitizers, Yb^{3+} and Nd^{3+} ions are frequently selected due to their high absorption cross-section (1.2 10^{-20} cm^2 at 980 nm and $\sim 10^{-19}$ cm^2 at 810 nm respectively) (Nadort et al., 2016; Kushida et al., 1968). The 980 nm excitation light for Yb^{3+} is absorbed by water and causes heat damage to biological samples, a problem that is mitigated with Nd^{3+} ions that have multiple absorption peaks at 730, 808, and 865 nm (Kushida et al., 1968).

Nd^{3+}, Ho^{3+}, Pr^{3+}, Tm^{3+}, and Er^{3+} have been used as activators with NIR luminescence centers at 1060 nm, 1155 nm, 1289 nm, 1475 nm, and 1525 nm peaks, respectively (Figure 3F) (Fan and Zhang, 2019). For example, Er and Yb-doped $NaCeF_4$ nanocrystals were synthesized by high-temperature co-precipitation methods and exhibit intense 1530 nm NIR emission with a maximum PL QY of 32.8% upon excitation at 980 nm (Lei et al., 2018).

Although other reviews have covered recent advances in downconverting NIR-emitting La NPs, a significant remaining issue is their relatively low absorption coefficient (Nadort et al., 2016; Fan and Zhang, 2019; Bünzli, 2010). The absorption coefficient of La NPs are still typically lower than organic dyes and other nanoparticles by several orders of magnitude; for example, the collective absorption coefficient of $NaCeF_4$ NP doped with 20% Yb and 1% Er (core diameter = 7 nm) is approximately 2000 $M^{-1}cm^{-1}$ at 980 nm (Lei et al., 2018) in comparison to $\sim 10^4$ $M^{-1}cm^{-1}$ (organic dye) and $\sim 10^5$ $M^{-1}cm^{-1}$ (QD). To overcome the weak light-absorbing characteristics of La NPs, exogenous organic dyes and QDs can be added to the La NP surface to harvest the excitation light in a broader wavelength range. This energy is then transferred to sensitizer ions, creating an "antenna effect" (Xie et al., 2017). This antenna effect has been demonstrated by combining surface-immobilized IR dyes (Figure 3G) (Zou et al., 2012) and biocompatible indocyanine green (ICG) dye (Shao et al., 2016) to the increased absorptivity of La NPs. More recently, Ag_2S (Zhang et al., 2020a) and Ag_2Se QDs (Song et al., 2019) have been also employed as antennas for La NPs, leading to QD-LaNP complexes with a higher absorption coefficient and greater photostability than their counterparts with organic dye-based antennas.

Improving quantum yield and fluorescence lifetime modulation

Due to their separated absorption (sensitizer) and luminescence (activator) centers, La NPs exhibit a large Stokes shift and tunable radiative pathway controlled by the distance and location of lanthanide ions in nanocrystals. Downconversion La NPs have been studied less than upconverting La NPs, but in current technologies, the PL QY of downconverting La NPs has shown PL QY ranging from 1% to 30%, which is higher than that of organic dyes and SWCNT and similar to that of NIR QDs (Table 1).

Compared with their s- and p-orbitals, the f-orbitals in lanthanide ions are strongly shielded and therefore behave as inner, rather than valence, electrons with narrow excitation and emission bands (Vogler and Kunkely, 2006). These parity-forbidden f-f transitions exhibit long lifetimes ranging from sub-milliseconds to milliseconds. These long lifetimes enable facile time-gated PL measurements, drastically improving signal-to-background ratios by removing short-lived emission and scattered excitation light (Tan et al., 2018). In addition, Fan et al. reported that the controlled activator concentration and the thickness of the energy relay layer can tune the emission lifetime of Ho and Er emitting La NPs spanning three orders of magnitude with a single NIR emission band (Figure 3H) (Fan et al., 2018). Increasing the thickness of interlayers that relay energy between the sensitizer and activator in multi-shell La NPs can tune the emission lifetime from 0.04 ms to 7 ms. This enables time-domain multiplexing, which spatially resolves the multiple nanoparticles by their specific emission lifetime.

Photostability

Because their absorption and radiation pathways originate from a shielded f-f transition that is insensitive to the environment, La NPs exhibit no blinking and have exceptionally photostable PL under modest laser

excitation. For example, Yb^{3+}- and Er^{3+}-doped $NaYF_4$ nanocrystals showed no fluctuation or photobleaching of their upconverted PL at individual and ensemble levels under a modest continuous laser power of 5×10^6 W/cm^2 at 980 nm (Wu et al., 2009). The photostability of NIR-emitting downconverting La NPs has not been investigated extensively compared with upconverted La NPs (Wu et al., 2009; Dang et al., 2016), but it is expected that their photostability will be similar due to a shared nanostructure and optical pathways. The chemical stability of La NPs is generally superior to the chemical stability of inorganic QDs; for example, host material $NaYF_4$ has reported extraordinary chemical stability (Wu et al., 2009; Dang et al., 2016; Qu et al., 2020).

NIR FLUORESCENT PROTEINS

For certain biological applications, the use of chemical or abiotic fluorescent probes is desirable; however, genetically encoded fluorescent reporters offer a number of advantages including cell specificity and tissue-targeted expression via viral vector delivery. Therefore, it is not surprising that in recent years there has been a focus on the development of NIR fluorescent proteins to, as with other NIR probes, take advantage of the tissue transparency window and extend multiplexing capabilities.

Although some naturally occurring protein systems make use of chromophores with absorption maxima well into the NIR range, they are typically not easy to adapt for use as fluorescent reporters. For example, the P870 and P960 bacterial reaction centers have maxima at 870 and 960 nm, respectively (Blankenship, 1994). Although typically non-fluorescent, they can be made so by inactivation of their photochemical pathways; however, they are far red-shifted due to strong coupling of two chromophores. In addition, as multi-component membrane-bound proteins, they are not easily engineered into workable reporters. Importantly, they also contain components that are not synthesized by animal cells, which are the typical end targets for these proteins. In fact, although Fischer and Lagarias successfully engineered a cyanobacterial phytochrome for intense fluorescence at 672 nm in 2004, the necessity to provide additional machinery to produce the chromophore in animal cells has prevented widespread use as a template for further engineering (Fischer and Lagarias, 2004). As such, most current NIR proteins are based on bacterial phytochromes that make use of biliverdin as the chromophore, a pigment naturally available to cells as a product of heme breakdown. Shu et al. demonstrated the first successful expression of such a system in 2009 (Shu et al., 2009). Since then, dozens of proteins have been engineered to improve upon and extend the capabilities of this first demonstration.

Limitations and advancements in NIR protein engineering

Red-shifting absorption and emission

As NIR proteins need to be expressed in cells, their primary engineering limitations are the constraints of the native capabilities of the cell and the requirement to use a genetically tractable model organism. For this reason, as stated earlier, although there are examples of naturally occurring chromophores far into the near-infrared, their versatility is highly restricted. The engineering challenge is then to attempt work within the constraints provided by the target system of interest. Bacterial phytochromes have primarily been used as a template as they provide the most straightforward model from which to work. It is therefore of some interest to discuss the structure and function of these proteins.

As the phytochromes that exist across algae, plants, and cyanobacteria, bacterial phytochromes are generally thought of as red light receptors, able to interconvert between a red and a far-red absorbing state (Auldridge and Forest, 2011). This process is controlled by an isomerization reaction around the central chromophore (Chernov et al., 2017). Notably, the maximum absorbance of the far-red state is Stokes shifted by ~70 nm, out to about 770 nm; however, the fluorescent population of phytochromes is usually not able to undergo the photochemical reaction to bring about the transition. In the generation of a more stable population of fluorescent phytochromes, the protein domains are truncated to make the transition unfavorable and stabilize the red-state, with mutations also designed to change the chromophore environment (Auldridge et al., 2012).

Due to the use of a naturally occurring chromophore, and the necessity for a large number of structural modifications to the protein it binds with, the number of possible further mutations to modify chromophore absorption becomes limited. One possible future approach to address this would be to seek stabilization of the far-red phytochrome state instead, using structure-driven rational
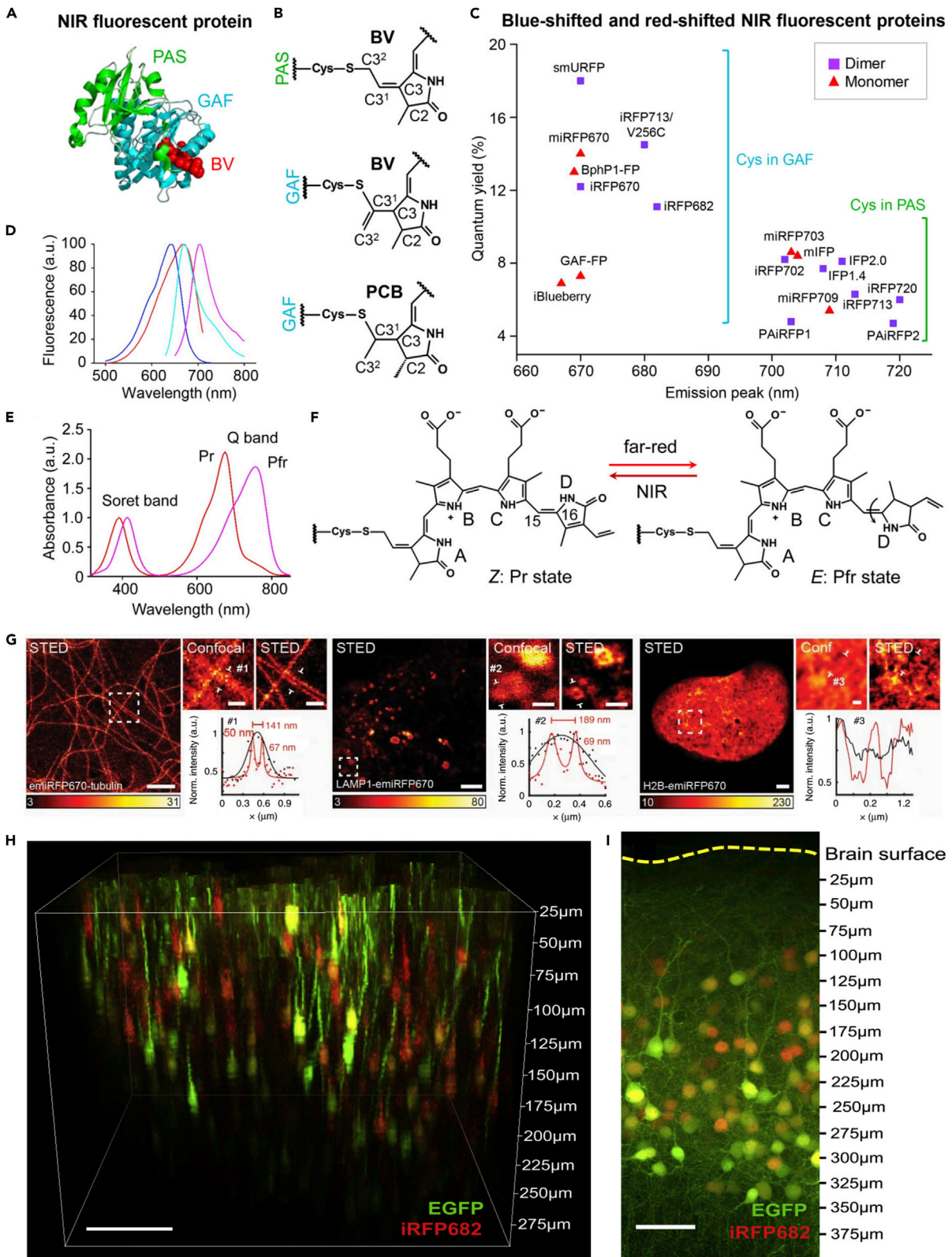
Figure 4. NIR-emitting proteins

(A) Structure of a two-domain NIR protein with PAS (Per–ARNT–Sim) and GAF (cGMP phosphodiesterase–adenylate cyclase–FhlA) domains shown, along with BV (biliverdin). The third domain of the protein is truncated.

(B) Chemical structures of BV or PCB (phycocyanobilin) bound to Cys residues in the PAS or GAF domains.

(C) Binding of BV to Cys residues in the GAF domain causes blue shifting of fluorescence. Squares represent dimeric proteins, whereas triangles represent monomers.

(D) Typical excitation and emission spectra for proteins with a Cys residue in the PAS domain (ex. red, em. magenta) or GAF domain (ex. blue, em. cyan).

(E) Absorption spectra of phytochromes in red or far-red states.

(F) Reversible isomerization reaction of BV that drives the transition between the two states.

(G) Confocal and STED images with a line profile along the indicated section of HeLa cells expressing an emiRFP670-tubulin fusion (left), U2OS cells expressing a LAMP1-emiRFP670 fusion (center), and U2OS cells expressing an H2B-emiRFP670 fusion (right). Scale bars are 2 μm for the full images and 500 nm for the inserts showing the zoomed-in regions of interest.

(H) *In vivo* two-photon imaging of iRFP682 in-mouse cortex acquired with 6.5 mW 880 nm excitation. Volumetric view of EGFP and iRFP682-expressing neurons in layers 1 and 2/3 of a mouse cortex. Scale bar 100 μm.

(I) Confocal images acquired from a fixed slice of the region in (H) acquired with 488 nm and 637 nm excitation. Scale bar 50 μm. Panels A–F are reproduced from (Chernov et al., 2017); Copyright 2017, American Chemical Society. Panel G is reproduced from (Matlashov et al., 2020); Copyright 2020, Springer Nature. Panels H and I are reproduced from (Piatkevich et al., 2017); Copyright 2017 Biophysical Society.

mutagenesis, although any such work has yet to be demonstrated. At the cost of increased complexity, another approach would be to integrate exogenous dyes or chromophores with proteins of interest. For example, Zeng et al. demonstrated the complex of H2a-4T dye with fetal bovine serum proteins and Cetuximab to perform image-guided photothermal therapy of cancer in mice, in the NIR-II window (Zeng et al., 2018).

Monomeric versus dimeric

At the most general level the population of near-infrared proteins can be categorized into two groups: monomeric or dimeric. The first demonstration by Shu et al. falls into the latter category, heading a category of proteins now referred to as infrared fluorescent proteins (IFPs). In this case, the dimerism was generally seen as a disadvantage, and their final product, IFP1.4, showed more propensity to monomeric behavior. Subsequent efforts worked to improve brightness and specificity of biliverdin for the protein. IFP2.0 was shown to be roughly 13x brighter and has been imaged in D*rosophila* larvae and mouse brain tissue, with monomeric propensity (Yu et al., 2014). IFPs have excitation maxima in the 680–690 nm range, with emission maxima at around 708 or 711 nm.

The second group of dimeric proteins are known as infraRed fluorescent proteins (iRFPs). These were developed using a different bacterial phytochrome as a template, from *Rhodospirillum centenum*, and variants were engineered with emission wavelengths between 670 nm and 720 nm (the most red-shifted of the dimeric proteins), with 1–2x brightness compared with IFPs (Shcherbakova and Verkhusha, 2013). A small number of photoactivatable proteins have also been produced for selective imaging or potentially super-resolution microscopy techniques, derived from a different bacterial phytochrome (Piatkevich et al., 2013).

In contrast, for many applications, (exclusively) monomeric proteins are preferred, particularly if fusion partners are involved for tracking studies. These more recent developments have been mostly derived from the previous dimeric versions with generally similar optical properties. Matlashov et al. recently demonstrated monomerization of the iRFPs, yielding the set of miRFPs, and some enhanced counterparts, emiRFPs (Matlashov et al., 2020). They furthermore demonstrated the ability to do two-color STED imaging with these proteins in cells and mice (Figure 4G). Their furthest red-shifted variant miRFP703 had an emission maximum at 703 nm. In the previous work from the Verkhusha group though, Shcherbakova et al. demonstrated miRFP709 with a maximum of 709 nm. Hodgson and colleagues were able to produce the furthest red-shifted monomeric iRFP, miRFP720, with a 720 nm emission maximum (Shcherbakova et al., 2018). In addition, they demonstrated its compatibility as an FRET pair with miRFP670. IFP2.0 has also been engineered into a fully monomeric form, mIFP2.0 (Yu et al., 2015). Recently, Ollinyk et al. demonstrated a new model template for monomeric proteins (Oliinyk et al., 2019). Using a single domain of a cyanobacteriochrome, they were able to produce the smallest monomeric fluorescent protein, named miRFP670nano, which is unrelated to the miRFPs described above. At 17 kDa, it is over 1.5x smaller than GFP-like fluorescent proteins, and is therefore a useful fusion partner, and can be used as a FRET donor for further red-shifted proteins.

Brightness versus emission wavelength

	Excitation Wavelength (nm)	Emission Wavelength (nm)	Quantum Yield (%)	Extinction (M^{-1} cm^{-1})	Brightness versus iRFP (%)
Dimeric proteins					
IFP1.4	684	708	7	92,000	8
IFP2.0	688	709	6.88	72,900	80
iRFP670	643	670	12.2	114000	225
iRFP682	663	682	11.1	90,000	162
iRFP702	673	702	8.2	93,000	124
iRFP	690	713	6.3	98,000	100
iRFP720	702	720	6	96,000	93
Monomeric proteins					
miRFP670	642	670	14	87,400	198
miRFP670-2	643	670	13.6	103000	227
miRFP680	661	680	14.5	94,000	221
miRFP682	663	682	11.2	91,000	165
miRFP702	673	703	8.1	88,000	115
miRFP703	674	703	8.6	90,900	127
miRFP709	683	709	5.4	78,400	77
miRFP713	690	713	7	99,000	112
miRFP720	702	720	6.1	98,000	97
mIFP2.0	683	705	6.9	65,900	111
miRFP670nano	645	670	10.8	95,000	167
emiRFP670	642	670	14	870700	198
emiRFP703	674	703	8.6	90,900	127
Wi-Phy	701	719	4.7	92,991	7

Applications

In the past five years, the emergence of NIR proteins has seen their application to a variety of biological fields, from cancer to neuroscience. They have also been integrated into more advanced imaging methodologies, such as FRET (Shcherbakova et al., 2018; Oliinyk et al., 2019), BRET (Rumyantsev et al., 2016), and super-resolution techniques such as STED (Kamper et al., 2018; Matlashov et al., 2020). The development of photoactivatable NIR proteins is promising for future demonstrations of techniques such as PALM, STORM, and RESOLFT as well. NIR proteins have been of particular utility in applications requiring multiplexing with existing architectures in the visible range, such as multi-channel imaging or optogenetics (Shemetov et al., 2017).

Background reduction and highly multiplexed imaging

The broad absorption and emission bands of fluorescent proteins have traditionally limited the number of simultaneous channels that can be acquired without fully spectrally resolved detection and deconvolution. NIR proteins have been shown to allow for multi-channel imaging, both among themselves, and with fluorescent proteins in the visible range. Donnelly et al. used miRFP703 in 4-channel imaging, as well as an additional FRET assay to study the role of Rac3 in breast cancer invasion and metastasis (Donnelly et al., 2017). In developing their NIR fluorescent protein, smURFP based on an allophycocyanin, Rodriguez et al. developed a cell cycle indicator using the further red-shifted IFP2.0 as well (Rodriguez et al., 2016). Shcherbakova et al. similarly demonstrated this capability using miRFPs (Shcherbakova et al., 2016). In the same study, they demonstrated the capability of producing three channel SIM super-resolution images across the visible and NIR and the ability to split these proteins to produce a reporter for protein-protein interactions. Telford et al. have also demonstrated the ability to do simultaneous red/NIR-excitation-based cell sorting using the iRFP family (Telford et al., 2015). Janssen et al. used multi-channel imaging with mRFP, GFP, and miRFP to study how myosin-V is involved in immobilization of cargo transport along the axon (Janssen et al., 2017).

Table 1. Comparison of properties of NIR luminescent materials

	Size	Absorption spectrum	Absorption coefficient (M^{-1} cm^{-1})	PLQY (%)	Photo-stability	Fluorescence wavelength tunability	Lifetime
SWNT	>0.1 μm (length) ∼1 nm (diameter)	Discrete bands	$>10^7$	0.01–0.1	+++++	High[a]	10–100 ps
La NP	10–50 nm	Discrete bands	10^3–10^4	1–30	+++++	Low	μs–ms
∼QD	2–10 nm	Broad bands	10^5	1–100	+++	High	ns–μs
Organic dye	∼1 nm	Discrete bands	10^5	0.3–6	++	Medium	0.1–100 ns
Protein	1–3 nm	Discrete bands	10^4–10^5	4–14	++	Low	∼0.5–1 ns

[a]Fluorescence wavelength is determined by chirality of SWNT; however, chirally pure SWNT has not been fully established commercially.

Neuroimaging and optogenetics

Many neuroscientists have turned to NIR proteins, particularly as the quest continues for high-resolution imaging deeper and deeper into the brain. These proteins' far-shifted absorption spectra also make them well suited for use in combination with the blue wavelengths typically used for optogenetic stimulation. Piatkevich et al. extensively characterized the viability of using iRFPs under two-photon excitation in neurons (Figures 4H and 4I) (Piatkevich et al., 2017). Richie et al. also demonstrated the feasibility of using iRFP713 as a reporter protein across sub-cellular locations in neurons, as well as its viability for use as a transgenic Cre-reporter for functional studies (Richie et al., 2017). Weinhard et al. used iRFP in conjunction with light-sheet microscopy and correlative light electron microscopy to study the microglial-mediated remodeling of synapses (Weinhard et al., 2018). Qian et al. also engineered a novel NIR genetically encoded Ca^{2+} indicator based on mIFP, demonstrating its usability in cultured cells and brain tissue (Qian et al., 2019).

A number of advances have also been made in the use of NIR fluorescent proteins, and NIR wavelengths generally, in optogenetics. In their report of miRFP720, Shcherbakova et al. demonstrated the compatibility of their NIR FRET-based biosensor with the blue-green LOV-TRAP optogenetic system (Shcherbakova et al., 2018). Roman et al. used iRFP713 to track nuclear motion and sequestration upon muscle contraction with optogenetic stimulation (Roman et al., 2017). Other research has focused instead on how to produce NIR controllable optogenetic tools, which would be compatible with existing blue-green technologies. Kaberniuk et al. engineered an NIR optogenetic system based on a bacterial phytochrome BphP1 and its binding partner PpsR2, which showed control of cell morphology and gene expression under 740 nm and 780 nm excitation (Kaberniuk et al., 2016). Redchuk et al. demonstrated that a similar system based on a BphP1-QPAS1 pair could induce gene transcription similarly to a blue-light system, LightOn (Redchuk et al., 2018). This work also showed that it could be used simultaneously with another blue-light system, LOV.

NIR LIGHT SOURCES AND DETECTION

As NIR optical probes have developed, there has been a concurrent search for new materials for light sources that can take advantage of the NIR spectral window. Since their first demonstration in the early 1980s, Ti:Sapphire lasers have been widely adopted as the NIR solid state laser standard, particularly for pulsed laser applications, due to their relatively broad tunability in the NIR. However, new laser technologies can now push the wavelength tuning range out to 2000 nm and beyond, produce supercontinuum sources, and provide nanostructured solutions for photonic circuitry and biomedical applications. Advances in fiber technologies have focused on increased bandwidth and amplification for communication purposes, as well as on new materials better suited to addressing specific biological or clinical problems. Additional work has focused on the development of broadband incoherent sources, particularly for compact, low-cost spectroscopy applications.

Fiber lasers

Demand for increased optical communication bandwidth and transmission rates, and for compact laser systems for biological and clinical applications, has continued to drive the development of new fiber laser and amplifier materials. For the division multiplexing techniques, especially the popular wavelength division multiplexing (WDM), that are used for optical communication, large bandwidth luminescent fiber materials are needed to provide sufficient optical power over all transmission bands. Recent work has focused

on extending the capabilities of the popular Er^{3+}-Doped Fiber Amplifiers (EDFA) through the introduction of additional rare earth ions. Chu et al. improved on Er^{3+}-doped bismuth borosilicate glasses by the additional codoping of Ce^{3+} and Yb^{3+}, producing a broadband luminescent material with a full-width-half-max (FWHM) of ~80 nm, and a reduction in undesirable up-conversion emission and excited state absorption (Chu et al., 2016). Dan and colleagues demonstrated a Nd^{3+}-Bi^+-Er^{3+} co-doped silica glass with ultra-broadband NIR luminescence of 600 nm FWHM from 1000 to 1600 nm, covering all transmission bands (Dan et al., 2019). Subsequently, they investigated the use of Y^{3+} for the enhancement of luminescence from Bi^+-Er^{3+} co-doped fibers (Dan et al., 2020). Other investigations have focused on the integration or adoption of entirely new materials. Cheng and colleagues demonstrated a simplified manufacture of a glass-based PbSe quantum dot fiber amplifier (QDFA), with double the FWHM and roughly half the level of noise of conventional EDFAs currently available (Cheng et al., 2020).

The integration of optically active nanostructures as pulsed lasers has also been pursued for a variety of applications. Ming et al. used PbS/CdS core/shell quantum dots as saturable absorbers to produce a candidate for tunable passively mode-locked Er^{3+}-doped fiber lasers (Ming et al., 2018). Cheng et al. similarly used the novel transition-metal dichalcogenide $PdTe_2$, to produce a passively Q-switched Yb^{3+}-doped fiber laser operating at 1066 nm (Cheng et al., 2019). Using carbon nanotubes as the saturable absorber, Meng et al. demonstrated a mode-locked thulium fiber laser with a 200 nm tuning range covering 1860–2060 nm (Meng et al., 2017). In addition to optical communications, thulium fiber lasers have been increasingly adopted for surgery applications, in particular for urology, due to the strong absorption of water at their operational wavelengths (Fried and Irby, 2018).

Nanowire lasers and detectors

Nanostructured light sources open many exciting avenues for the development of on-chip systems and nanophotonic circuitry for a variety of applications. In particular, nanowire lasers appear to be especially promising for their ability to provide guided coherent light in extremely compact geometries—often just microns along the long axis and hundreds of nm along the short. Two remaining challenges, however, are the manufacturing of nanowire lasers at longer NIR wavelengths and lasing at temperatures close to room temperature. A number of material compositions and manufacturing techniques have been proposed to overcome these issues. Ren et al. presented a GaAsSb nanowire with high Q factor lasing and a relatively high characteristic temperature of 129 K, with an emission wavelength tunable from 890 to 990 nm based on the relative Sb composition of the lattice (Ren et al., 2018). Chen et al. manufactured a GaAs/GaNAs/GaAs multishell nanowire with emission at 1000 nm and an estimated characteristic temperature of 160 K (Chen et al., 2019). Efforts to produce NIR organic lasers are typically hampered by intrinsic non-radiative processes, dictated by the energy gap law. Recently, Wu et al. took advantage of the excited-state intramolecular proton transfer process between the enol and keto forms of the compound (E)-3-(4-(dimethylamino)phenyl)-1-(1-hydroxynaphthalen-2-yl)prop-2-en-1-one (DMHC) to overcome this barrier and demonstrate a single-crystal organic nanowire laser (Wu et al., 2020).

The NIR optical properties of nanowire structures have also been investigated more generally for optoelectronic and detection applications and for use in absorption-based imaging and medical technologies. Li et al. first demonstrated broadband photoluminescence from silicon nanowires across the visible and NIR (500–920 nm) under 980 nm CW illumination, with potential applications from biosensors to an optical source in itself (Li et al., 2018b). Zheng et al. demonstrated the possibility to use p-type SnS and SnSe nanowires as NIR photodetectors with sub-ms response (Zheng et al., 2018). More recently, Sb_2Se_3 nanowires have been used to produce similarly rapid photodetectors for the visible through NIR. These crystalline nanowires exhibit strong anisotropy, yielding a highly polarization sensitive detector (Ma et al., 2019). The strong absorption of some nanowire substrates in the near IR has also made them useful targets for photothermal therapies. For example, Au-coated Si nanowires have been demonstrated as suitable for photothermal treatment of cancer cells (Convertino et al., 2018).

LEDs

In contrast to most lasers, light-emitting diodes (LEDs) tend to be more portable, cost-effective, and safer to use for a variety of applications ranging from NIR spectroscopy to light therapies. Similar to organic solid state lasers, traditional NIR LED technologies have often focused on semiconductors due to the high non-radiative decay of organic compounds in the NIR. In recent years, significant work has been done to expand

the set of materials available for LEDs, while also producing extremely broadband sources for spectroscopy and imaging across the NIR window.

Recent work has demonstrated the possibility of manufacturing organic LEDs operating in the NIR. Hu et al. designed exciplex-based OLED materials with NIR emission at either 704 or 730 nm based on combinations of a novel synthesized fluorescent compound and commercially available materials (Hu et al., 2020). Zhang et al. improved on existing Ir(III) complexes, which have been used previously to produce mixed red/NIR emission, by demonstrating Ir(III) based OLED with complete emission in the NIR, centered at 850 nm (Zhang et al., 2020b). Similarly, Wei et al. improved on existing Pt(II) organometallic complexes producing NIR emission between 866 and 960 nm, with a record photoluminescence quantum yield of 5%–12%, through exciton delocalization over numerous molecules (Wei et al., 2020).

Substantial improvements in phosphor-converted LEDs for broadband NIR emission have also been realized in recent years. Numerous Cr^{3+}-based phosphors have been designed, usually used in conjugation with a blue LED for excitation, often with NIR photoluminescence yields of >65%, broadband emission over 700–1100 nm, and high thermal stability. Output powers in the 10s of mW make these LEDs suitable for a variety of near infrared spectroscopy applications (Shao et al., 2018a, 2018b; Xu et al., 2020; Rajendran et al., 2019). Basore et al. have also demonstrated Cr^{3+}:garnet LED with 98.6% internal quantum efficiency and high power emission of over 750 mW over the 700–1000 nm range (Basore et al., 2020). Most recently, Eu^{2+}-doped phosphors have also been used to produce broadband LEDs covering the visible and NIR (Lai et al., 2020; Tang et al., 2020).

FUTURE DIRECTIONS AND PERSPECTIVES

Over the past several years, the development of new NIR-emitting materials has rapidly expanded due to a growing understanding of the structural and material characteristics that underpin their luminescent properties. In particular, NIR materials have enabled better control over stability, quantum yield, and tunability of material performance in complex environments for applications in biology, as optical light sources, and in detectors.

New molecular engineering techniques have expanded the traditional emission window for NIR-emitting organic dyes, particularly for small molecule dyes. As new molecular structures become easier to synthesize, dyes with higher QY, narrow emission wavelengths, and large Stokes shifts will be easier to achieve. In parallel, efforts toward carbon-based NIR emitters such as SWNTs and carbon dots have revealed exciting nonlinear optical properties that can be tuned through better control of material properties such as chirality and electronic doping. Similarly, inorganic nanomaterials including semiconducting quantum dots and lanthanide-based nanoparticles exhibit significantly higher QY while maintaining some degree of tunability through changes in material composition. However, there remain a number of areas that warrant further exploration, including the study of downconverting nanoparticles and improved absorption coefficients.

In this review, we have limited our focus to the use of nanomaterials in aggregate. However, nanomaterials also offer exciting possibilities in tracking single molecules and super-resolution imaging, with work still remaining to balance the need for smaller sizes with brightness and stability. In particular, SWNTs have been able to mitigate some of the challenges faced by molecular dyes and fluorescent proteins to enable single molecule tracking (Gao et al., 2017; Godin et al., 2019). Many of the properties highlighted in this review, including the narrow-band emission and size-tunable emission exhibited by quantum dots and upconverting nanoparticles, are ideal for super-resolution microscopy. We direct readers to other recent publications that provide a more comprehensive discussion of the use of nanoparticles in these applications (Jin et al., 2018).

As NIR luminescent materials are increasingly desired for biological imaging applications, new engineering tools can be leveraged to engineer NIR fluorescent proteins at smaller length scales and with an expanded emission window. This development is critical for applications such as multi-channel imaging and optogenetics and cell-specific targeting of NIR emitters. Likewise, new engineered materials have been recently developed for expansion of lasing, detection, and LED capabilities into the NIR spectrum. The interplay of these different material systems could allow researchers to overcome many of the existing barriers in the development of tools for NIR imaging. We hope this review will provide a fundamental understanding

of the underlying chemical and physical properties that govern NIR emission across this diverse range of materials, inspiring future efforts by researchers who seek to develop and use NIR-emitting materials.

ACKNOWLEDGMENTS

DECLARATION OF INTERESTS

The authors declare no competing interests.

REFERENCES

Algar, W.R. (2020). Heroes or villains? How nontraditional luminescent materials do and do not enhance bioanalysis and imaging. Chem. Mater. 32, 4863–4883.

Antaris, A.L., Robinson, J.T., Yaghi, O.K., Hong, G., Diao, S., Luong, R., and Dai, H. (2013). Ultra-low doses of chirality sorted (6,5) carbon nanotubes for simultaneous tumor imaging and photothermal therapy. ACS Nano 7, 3644–3652.

Antaris, A.L., Chen, H., Cheng, K., Sun, Y., Hong, G., Qu, C., Diao, S., Deng, Z., Hu, X., Zhang, B., et al. (2016). A small-molecule dye for NIR-II imaging. Nat. Mater. 15, 235–242.

Auldridge, M.E., and Forest, K.T. (2011). Bacterial phytochromes: more than meets the light. Crit. Rev. Biochem. Mol. Biol. 46, 67–88.

Auldridge, M.E., Satyshur, K.A., Anstrom, D.M., and Forest, K.T. (2012). Structure-guided engineering enhances a phytochrome-based infrared fluorescent protein. J. Biol. Chem. 287, 7000–7009.

Bachilo, S.M., Strano, M.S., Kittrell, C., Hauge, R.H., Smalley, R.E., and Weisman, R. (2002). Structure-assigned optical spectra of single-walled carbon nanotubes. Science 298, 2361–2366.

Bai, L., Sun, P., Liu, Y., Zhang, H., Hu, W., Zhang, W., Liu, Z., Fan, Q., Li, L., and Huang, W. (2019). Novel aza-BODIPY based small molecular NIR-II fluorophores for in vivo imaging. Chem. Commun. (Camb) 55, 10920–10923.

Basore, E.T., Xiao, W., Liu, X., Wu, J., and Qiu, J. (2020). Broadband near-infrared garnet phosphors with near-unity internal quantum efficiency. Adv. Opt. Mater. 8, 2000296.

Berger, F.J., Jan, L., Tim, N., Tobias, K., Sebastian, L., Lucas, K., Müller, C.C., Bongartz, L.M., Lumsargis, V.A., Zakharko, Y., et al. (2019). Brightening of long, polymer-wrapped carbon nanotubes by sp 3 functionalization in organic solvents. ACS Nano, https://doi.org/10.1021/acsnano.9b03792.

Bisker, G., Dong, J., Park, H.D., Iverson, N.M., Ahn, J., Nelson, J.T., Landry, M.P., Kruss, S., and Strano, M.S. (2016). Protein-targeted corona phase molecular recognition. Nat. Commun. 7, 10241.

Blankenship, R.E. (1994). Protein structure, electron transfer and evolution of prokaryotic photosynthetic reaction centers. Antonie van Leeuwenhoek 65, 311–329.

Bonis-O'Donnell, J.T., Page, R.H., Beyene, A.G., Tindall, E.G., McFarlane, I.R., and Landry, M.P. (2017). Dual near-infrared two-photon microscopy for deep-tissue dopamine nanosensor imaging. Adv. Funct. Mater. 27, 1702112.

Brozena, A.H., Kim, M., Powell, L.R., and Wang, Y. (2019). Controlling the optical properties of carbon nanotubes with organic colour-centre quantum defects. Nat. Rev. Chem. 3, 375–392.

Bruns, O.T., Bischof, T.S., Harris, D.K., Franke, D., Shi, Y., Riedemann, L., Bartelt, A., Jaworski, F.B., Carr, J.A., Rowlands, C.J., et al. (2017). Next-generation optical imaging with short-wave infrared quantum dots. Nat. Biomed. Eng. 1, https://doi.org/10.1038/s41551-017-0056.

Bünzli, J.-C.G. (2010). Lanthanide luminescence for biomedical analyses and imaging. Chem. Rev. 110, 2729–2755.

Carr, J.A., Franke, D., Caram, J.R., Perkinson, C.F., Saif, M., Askoxylakis, V., Datta, M., Fukumura, D., Jain, R.K., Bawendi, M.G., and Bruns, O.T. (2018). Shortwave infrared fluorescence imaging with the clinically approved near-infrared dye indocyanine green. Proc. Natl. Acad. Sci. U S A 115, 4465–4470.

Chen, S., Yukimune, M., Fujiwara, R., Ishikawa, F., Chen, W.M., and Buyanova, I.A. (2019). Near-infrared lasing at 1 μm from a dilute-nitride-based multishell nanowire. Nano Lett. 19, 885–890.

Cheng, P.K., Tang, C.Y., Wang, X.Y., Ma, S., Long, H., Tsang, Y.H., and Tsang, Y.H. (2019). Passively Q-switched ytterbium-doped fiber laser based on broadband multilayer platinum ditelluride (PtTe2) saturable absorber. Sci. Rep. 9, 10106.

Cheng, C., Wang, F., and Cheng, X. (2020). PbSe quantum-dot-doped broadband fiber amplifier based on sodium-aluminum-borosilicate-silicate glass. Opt. Laser Technol. 122, 105812.

Chernov, K.G., Redchuk, T.A., Omelina, E.S., and Verkhusha, V.V. (2017). Near-infrared fluorescent proteins, biosensors, and optogenetic tools engineered from phytochromes. Chem. Rev. 117, 6423–6446.

Chu, Y., Ren, J., Zhang, J., Peng, G., Yang, J., Wang, P., and Yuan, L. (2016). Ce(3+)/Yb(3+)/Er(3+) triply doped bismuth borosilicate glass: a potential fiber material for broadband near-infrared fiber amplifiers. Sci. Rep. 6, 33865.

Convertino, A., Mussi, V., Maiolo, L., Ledda, M., Lolli, M.G., Bovino, F.A., Fortunato, G., Rocchia, M., and Lisi, A. (2018). Array of disordered silicon nanowires coated by a gold film for combined NIR photothermal treatment of cancer cells and Raman monitoring of the process evolution. Nanotechnology 29, 415102.

Cosco, E.D., Caram, J.R., Bruns, O.T., Franke, D., Day, R.A., Farr, E.P., Bawendi, M.G., and Sletten, E.M. (2017). Flavylium polymethine fluorophores for near- and shortwave infrared imaging. Angew. Chem. Int. Ed. 56, 13126, https://doi.org/10.1002/ange.201706974.

Dan, H.K., Qiu, J., Zhou, D., Jiao, Q., Wang, R., and Le Thai, N. (2019). Super broadband near-infrared emission and energy transfer in Nd–Bi–Er Co-doped transparent silicate glass-ceramics. Mater. Lett. 234, 142–147.

Cosco, E.D., Spearman, A.L., Ramakrishnan, S., Lingg, J.G.P., Saccomano, M., Pengshung, M., Arús, B.A., Wong, K.C.Y., Glasl, S., Ntziachristos, V., et al. (2020). Shortwave infrared polymethine fluorophores matched to excitation lasers enable non-invasive, multicolour in vivo imaging in real time. Nat. Chem. https://doi.org/10.1038/s41557-020-00554-5.

Dan, H.K., Le, D.-N., Nguyen-Truong, H.T., Tap, T.D., Vinh, H.X., Ty, N.M., Wang, R., Zhou, D., and Qiu, J. (2020). Effects of Y3+on the enhancement NIR emission of Bi+-Er3+ Co-doped in transparent silicate glass-ceramics for erbium-doped fiber amplifier (EDFA). J. Lumin. 219, 116942.

Dang, X., Gu, L., Qi, J., Correa, S., Zhang, G., Belcher, A.M., and Hammond, P.T. (2016). Layer-by-Layer assembled fluorescent probes in the second near-infrared window for systemic delivery and detection of Ovarian cancer. Proc. Natl. Acad. Sci. U S A 113, 5179–5184.

Danné, N., Godin, A.G., Gao, Z., Varela, J.A., Groc, L., Lounis, B., and Cognet, L. (2018). Comparative analysis of photoluminescence and upconversion emission from individual carbon nanotubes for bioimaging applications. ACS Photon. 5, 359–364.

Ding, B., Xiao, Y., Zhou, H., Zhang, X., Qu, C., Xu, F., Deng, Z., Cheng, Z., and Hong, X. (2019). Polymethine thiopyrylium fluorophores with absorption beyond 1000 Nm for biological imaging in the second near-infrared subwindow. J. Med. Chem. *62*, 2049–2059.

Donnelly, S.K., Cabrera, R., Mao, S.P.H., Christin, J.R., Wu, B., Guo, W., Bravo-Cordero, J.J., Condeelis, J.S., Segall, J.E., and Hodgson, L. (2017). Rac3 regulates breast cancer invasion and metastasis by controlling adhesion and matrix degradation. J. Cell Biol. *216*, 4331–4349.

Efros, A.L., and Nesbitt, D.J. (2016). Origin and control of blinking in quantum dots. Nat. Nanotechnol. *11*, 661–671.

Escobedo, J.O., Rusin, O., Lim, S., and Strongin, R.M. (2010). NIR dyes for bioimaging applications. Curr. Opin. Chem. Biol. *14*, 64–70.

Fan, Y., and Zhang, Fan (2019). A new generation of NIR-II probes: lanthanide-based nanocrystals for bioimaging and biosensing. Adv. Opt. Mater. https://doi.org/10.1002/adom.201801417.

Fan, Y., Wang, P., Lu, Y., Wang, R., Zhou, L., Zheng, X., Li, X., Piper, J.A., and Zhang, F. (2018). Lifetime-engineered NIR-II nanoparticles unlock multiplexed in vivo imaging. Nat. Nanotechnol. *13*, 941–946.

Fischer, A.J., and Lagarias, J. (2004). Harnessing phytochrome's glowing potential. Proc. Natl. Acad. Sci. U S A *101*, 17334–17339.

Franke, D., Harris, D.K., Chen, O., Bruns, O.T., Carr, J.A., Wilson, M.W., and Bawendi, M.G. (2016). Continuous injection synthesis of Indium arsenide quantum dots emissive in the short-wavelength infrared. Nat. Commun. *7*, 12749.

Fried, N.M., and Irby, P.B. (2018). Advances in laser technology and fibre-optic delivery systems in lithotripsy. Nat. Rev. Urol. *15*, 563–573.

Gao, Z., Danné, N., Godin, A.G., Lounis, B., and Cognet, L. (2017). Evaluation of different single-walled carbon nanotube surface coatings for single-particle tracking applications in biological environments. Nanomaterials (Basel) 7, https://doi.org/10.3390/nano7110393.

Godard, A., Kalot, G., Pliquett, J., Busser, B., Le Guével, X., Wegner, K.D., Resch-Genger, U., Rousselin, Y., Coll, J.L., Denat, F., et al. (2020). Water-soluble aza-BODIPYs: biocompatible organic dyes for high contrast in vivo NIR-II imaging. Bioconjug. Chem. *31*, 1088–1092.

Godin, A.G., Setaro, A., Gandil, M., Haag, R., Adeli, M., Reich, S., and Cognet, L. (2019). Photoswitchable single-walled carbon nanotubes for super-resolution microscopy in the near-infrared. Science Advances *5*, eaax1166.

Gong, Y.J., Zhang, X.B., Mao, G.J., Su, L., Meng, H.M., Tan, W., Feng, S., and Zhang, G. (2016). A unique approach toward near-infrared fluorescent probes for bioimaging with remarkably enhanced contrast. Chem. Sci. *7*, 2275–2285.

Hong, G., Antaris, A.L., and Dai, H. (2017). Near-infrared fluorophores for biomedical imaging. Nat. Biomed. Eng. *1*, 0010.

Hu, Y., Yu, Y.J., Yuan, Y., Jiang, Z.Q., and Liao, L.S. (2020). Exciplex-based organic light-emitting diodes with near-infrared emission. Adv. Opt. Mater. *8*, 1901917.

Janssen, A.F.J., Tas, R.P., van Bergeijk, P., Oost, R., Hoogenraad, C.C., and Kapitein, L.C. (2017). Myosin-V induces cargo immobilization and clustering at the axon initial segment. Front. Cell Neurosci. *11*, 260.

Javaux, C., Mahler, B., Dubertret, B., Shabaev, A., Rodina, A.V., Efros, A.L., Yakovlev, D.R., Liu, F., Bayer, M., Camps, G., et al. (2013). Thermal activation of non-radiative auger recombination in charged colloidal nanocrystals. Nat. Nanotechnol. *8*, 206–212.

Jena, P.V., Safaee, M.M., Heller, D.A., and Roxbury, D. (2017). DNA-carbon nanotube complexation affinity and photoluminescence modulation are independent. ACS Appl. Mater. Interfaces 9, 21397–21405.

Jeong, S., Song, J., Lee, W., Ryu, Y.M., Jung, Y., Kim, S.Y., Kim, K., Hong, S.C., Myung, S.J., and Kim, S. (2017). Cancer-microenvironment-sensitive activatable quantum dot probe in the second near-infrared window. Nano Lett. *17*, 1378, https://doi.org/10.1021/acs.nanolett.6b04261.

Jin, D., Xi, P., Wang, B., Zhang, L., Enderlein, J., and van Oijen, A.M. (2018). Nanoparticles for super-resolution microscopy and single-molecule tracking. Nat. Methods 15, 415–423.

Kaberniuk, A.A., Shemetov, A., and Verkhusha, V.V. (2016). A bacterial phytochrome-based optogenetic system controllable with near-infrared light. Nat. Methods 13, 591–597.

Kamper, M., Ta, H., Jensen, N.A., Hell, S.W., and Jakobs, S. (2018). Near-infrared STED nanoscopy with an engineered bacterial phytochrome. Nat. Commun. *9*, 4762.

Kushida, T., Marcos, H.M., and Geusic, J.E. (1968). Laser transition cross section and fluorescence branching ratio forNd3 in yttrium aluminum garnet. Phys. Rev. https://doi.org/10.1103/physrev.167.289.

Kwon, H., Kim, M., Meany, B., Piao, Y., Powell, L.R., and Wang, Y. (2015). Optical probing of local pH and temperature in complex fluids with covalently functionalized, semiconducting carbon nanotubes. J. Phys. Chem. C 119, 3733–3739.

Kwon, H., Furmanchuk, A., Kim, M., Meany, B., Guo, Y., Schatz, G.C., and Wang, Y. (2016). Molecularly tunable fluorescent quantum defects. J. Am. Chem. Soc. *138*, 6878–6885.

Lai, S., Zhao, M., Qiao, J., Molokeev, M.S., and Xia, Z. (2020). Data-driven photoluminescence tuning in Eu2+-doped phosphors. J. Phys. Chem. Lett. *11*, 5680–5685.

Lei, Z., Li, X., Luo, X., He, H., Zheng, J., Qian, X., and Yang, Y. (2017). Bright, stable, and biocompatible organic fluorophores absorbing/emitting in the deep near-infrared spectral region. Angew. Chem. Int. Ed. *56*, 2979–2983.

Lei, X., Li, R., Tu, D., Shang, X., Liu, Y., You, W., Sun, C., Zhang, F., and Chen, X. (2018). Intense near-infrared-II luminescence from NaCeF4:Er/Yb nanoprobes for in vitro bioassay and in vivo bioimaging. Chem. Sci. https://doi.org/10.1039/c8sc00927a.

Lei, Z., Sun, C., Pei, P., Wang, S., Li, D., Zhang, X., and Zhang, F. (2019). Stable, wavelength-tunable fluorescent dyes in the NIR-II region for in vivo high-contrast bioimaging and multiplexed biosensing. Angew. Chem. Int. Ed. *131*, 8250–8255.

Li, B., Lu, L., Zhao, M., Lei, Z., and Zhang, F. (2018a). An efficient 1064 Nm NIR-II excitation fluorescent molecular dye for deep-tissue high-resolution dynamic bioimaging. Angew. Chem. Int. Ed. *130*, 7605–7609.

Li, Z., Wang, X., Liu, S., Yang, J., Shi, K., Wang, H., Zhu, D., and Xing, X. (2018b). Broadband photoluminescence of silicon nanowires excited by near-infrared continuous wave lasers. Opt. Laser Technol. *99*, 81–85.

Li, C., Chen, K., Guan, M., Wang, X., Zhou, X., Zhai, F., Dai, J., Li, Z., Sun, Z., Meng, S., et al. (2019a). Extreme nonlinear strong-field photoemission from carbon nanotubes. Nat. Commun. *10*, 4891.

Li, M., Chen, T., Gooding, J., and Liu, J. (2019b). Review of carbon and graphene quantum dots for sensing. ACS Sens. *4*, 1732–1748.

Li, Y., Bai, G., Zeng, S., and Hao, J. (2019c). Theranostic carbon dots with innovative NIR-II emission for in vivo renal-excreted optical imaging and photothermal therapy. ACS Appl. Mater. Interfaces *11*, 4737–4744.

Ma, Z., Chai, S., Feng, Q., Li, L., Li, X., Huang, L., Liu, D., Sun, J., Jiang, R., Zhai, T., et al. (2019). Chemical vapor deposition growth of high crystallinity Sb2 Se3 nanowire with strong anisotropy for near-infrared photodetectors. Small 15, e1805307.

Mann, F.A., Herrmann, N., Opazo, F., and Kruss, S. (2020). Quantum defects as a toolbox for the covalent functionalization of carbon nanotubes with peptides and proteins. Angew. Chem. Int. Ed. https://doi.org/10.1002/anie.202003825.

Matlashov, M.E., Shcherbakova, D.M., Alvelid, J., Baloban, M., Pennacchietti, F., Shemetov, A.A., Testa, I., and Verkhusha, V.V. (2020). A set of monomeric near-infrared fluorescent proteins for multicolor imaging across scales. Nat. Commun. *11*, 239.

Meng, Y., Li, Y., Xu, Y., and Wang, F. (2017). Carbon nanotube mode-locked thulium fiber laser with 200 Nm tuning range. Sci. Rep. *7*, 45109.

Ming, N., Tao, S., Yang, W., Chen, Q., Sun, R., Wang, C., Wang, S., Man, B., and Zhang, H. (2018). Mode-locked Er-doped fiber laser based on PbS/CdS core/shell quantum dots as saturable absorber. Opt. Express 26, 9017–9026.

Moreels, I., Justo, Y., De Geyter, B., Haustraete, K., Martins, J.C., and Hens, Z. (2011). Size-tunable, bright, and stable PbS quantum dots: a surface chemistry study. ACS Nano 5, 2004–2012.

Nadort, A., Zhao, J., and Goldys, E.M. (2016). Lanthanide upconversion luminescence at the nanoscale: fundamentals and optical properties. Nanoscale 8, 13099–13130.

Nißler, R., Mann, F.A., Preiß, H., Selvaggio, G., Herrmann, N., and Kruss, S. (2019). Chirality enriched carbon nanotubes with tunable wrapping via corona phase exchange purification (CPEP). Nanoscale 11, 11159–11166.

Oliinyk, O.S., Shemetov, A.A., Pletnev, S., Shcherbakova, D.M., and Verkhusha, V.V. (2019). Smallest near-infrared fluorescent protein evolved from cyanobacteriochrome as versatile tag for spectral multiplexing. Nat. Commun. 10, 279.

Pan, J., Li, F., and Choi, J.H. (2017). Single-walled carbon nanotubes as optical probes for bio-sensing and imaging. J. Mater. Chem. B 5, 6511–6522.

Park, Y., Jeong, S., and Kim, S. (2017). Medically translatable quantum dots for biosensing and imaging. J. Photochem. Photobiol. C Photochem. Rev. 30, 51–70.

Piao, Y., Meany, B., Powell, L.R., Valley, N., Kwon, H., Schatz, G.C., and Wang, Y. (2013). Brightening of carbon nanotube photoluminescence through the incorporation of sp3 defects. Nat. Chem. 5, 840–845.

Piatkevich, K.D., Subach, F.V., and Verkhusha, V.V. (2013). Far-red light photoactivatable near-infrared fluorescent proteins engineered from a bacterial phytochrome. Nat. Commun. 4, 2153.

Piatkevich, K.D., Suk, H.J., Kodandaramaiah, S.B., DeGennaro, E.M., Drobizhev, M., Hughes, T.E., Desimone, R., Boyden, E.S., and Verkhusha, V.V. (2017). Near-infrared fluorescent proteins engineered from bacterial phytochromes in neuroimaging. Biophys. J. 113, 2299–2309.

Pinals, R.L., Chio, L., Ledesma, F., and Landry, M.P. (2020). Engineering at the nano-bio Interface: harnessing the protein corona towards nanoparticle design and function. Analyst 145, 5090–5112.

Qian, G., Gao, J.P., and Wang, Z.Y. (2012). Near-infrared chemiluminescence tunable from 900 nm to 1700 nm from narrow-bandgap compounds and polymers. Chem. Commun. (Camb). https://doi.org/10.1039/c2cc32624h.

Qian, Y., Piatkevich, K.D., Mc Larney, B., Abdelfattah, A.S., Mehta, S., Murdock, M.H., Gottschalk, S., Molina, R.S., Zhang, W., Chen, Y., et al. (2019). A genetically encoded near-infrared fluorescent calcium ion indicator. Nat. Methods 16, 171–174.

Qu, Z., Shen, J., Li, Q., Xu, F., Wang, F., Zhang, X., and Fan, C. (2020). Near-IR emissive rare-earth nanoparticles for guided surgery. Theranostics 10, 2631–2644.

Rajendran, V., Lesniewski, T., Kaczmarek, Wei-Kong Pang, Mahlik, S., Grinberg, M., Leniec, G., Kaczmarek, S.M., Pang, W.-K., Lin, Y.-S., Lu, K.-M., Lin, C.-M., et al. (2019). Ultra-broadband phosphors converted near-infrared light emitting diode with efficient radiant power for spectroscopy applications. ACS Photon. 6, 3215–3224.

Redchuk, T.A., Kaberniuk, A.A., and Verkhusha, V.V. (2018). Near-infrared light-controlled systems for gene transcription regulation, protein targeting and spectral multiplexing. Nat. Protoc. 13, 1121–1136.

Ren, D., Ahtapodov, L., Nilsen, J.S., Yang, J., Gustafsson, A., Huh, J., Conibeer, G.J., van Helvoort, A.T.J., Fimland, B.O., and Weman, H. (2018). Single-mode near-infrared lasing in a GaAsSb-based nanowire superlattice at room temperature. Nano Lett. 18, 2304–2310.

Richie, C.T., Whitaker, L.R., Whitaker, K.W., Necarsulmer, J., Baldwin, H.A., Fortuno, L., Hinkle, J.J., Koivula, P., Henderson, M.J., Sun, W., et al. (2017). Near-infrared fluorescent protein iRFP713 as a reporter protein for optogenetic vectors, a transgenic cre-reporter rat, and other neuronal studies. J. Neurosci. Methods 284, 1–14.

Rodriguez, E.A., Tran, G.N., Gross, L.A., Crisp, J.L., Shu, X., Lin, J.Y., and Tsien, R.Y. (2016). A far-red fluorescent protein evolved from a cyanobacterial phycobiliprotein. Nat. Methods 13, 763–769.

Roman, W., Martins, J.P., Carvalho, F.A., Voituriez, R., Abella, J.V.G., Santos, N.C., Cadot, B., Way, M., and Gomes, E.R. (2017). Myofibril contraction and crosslinking drive nuclear movement to the periphery of skeletal muscle. Nat. Cell Biol. 19, 1189–1201.

Roxbury, D., Jena, P.V., Williams, R.M., Enyedi, B., Niethammer, P., Marcet, S., Verhaegen, M., Blais-Ouellette, S., and Heller, D.A. (2015). Hyperspectral microscopy of near-infrared fluorescence enables 17-chirality carbon nanotube imaging. Sci. Rep. 5, 14167.

Rumyantsev, K.A., Turoverov, K., and Verkhusha, V.V. (2016). Near-infrared bioluminescent proteins for two-color multimodal imaging. Sci. Rep. 6, 36588.

Salem, D.P., Landry, M.P., Bisker, G., Ahn, J., Kruss, S., and Strano, M.S. (2016). Chirality dependent corona phase molecular recognition of DNA-wrapped carbon nanotubes. Carbon 97, 147–153.

Santos, H.D.A., Zabala Gutiérrez, I., Shen, Y., Lifante, J., Ximendes, E., Laurenti, M., Méndez-González, D., Melle, S., Calderón, O.G., López Cabarcos, E., et al. (2020). Ultrafast photochemistry produces superbright short-wave infrared dots for low-dose in vivo imaging. Nat. Commun. 11, 2933.

Shao, W., Chen, G., Kuzmin, A., Kutscher, H.L., Pliss, A., Ohulchanskyy, T.Y., and Prasad, P.N. (2016). Tunable narrow band emissions from dye-sensitized core/shell/shell nanocrystals in the second near-infrared biological window. J. Am. Chem. Soc. 138, 16192–16195.

Shao, Q., Ding, H., Yao, L., Xu, J., Liang, C., and Jiang, J. (2018a). Photoluminescence properties of a ScBO3:Cr3+ phosphor and its applications for broadband near-infrared LEDs. RSC Adv. 8, 12035–12042.

Shao, Q., Ding, H., Yao, L., Xu, J., Liang, C., Li, Z., Dong, Y., and Jiang, J. (2018b). Broadband near-infrared light source derived from Cr. Chip. Opt. Lett. 43, 5251–5254.

Shcherbakova, D.M., and Verkhusha, V.V. (2013). Near-infrared fluorescent proteins for multicolor in vivo imaging. Nat. Methods 10, 751–754.

Shcherbakova, D.M., Baloban, M., Emelyanov, A.V., Brenowitz, M., Guo, P., and Verkhusha, V.V. (2016). Bright monomeric near-infrared fluorescent proteins as tags and biosensors for multiscale imaging. Nat. Commun. 7, 12405.

Shcherbakova, D.M., Cox Cammer, N., Huisman, T.M., Verkhusha, V.V., and Hodgson, L. (2018). Direct multiplex imaging and optogenetics of rho GTPases enabled by near-infrared FRET. Nat. Chem. Biol. 14, 591–600.

Shemetov, A.A., Oliinyk, O.S., and Verkhusha, V.V. (2017). How to increase brightness of near-infrared fluorescent proteins in mammalian cells. Cell Chem. Biol. 24, 758–766.e3.

Shi, J., Chu, H., Li, Y., Zhang, X., Pan, H., and Li, D. (2019). Synthesis and nonlinear optical properties of semiconducting single-walled carbon nanotubes at 1 μm. Nanoscale 11, 7287–7292.

Shu, X., Royant, A., Lin, M.Z., Aguilera, T.A., Lev-Ram, V., Steinbach, P.A., and Tsien, R.Y. (2009). Mammalian expression of infrared fluorescent proteins engineered from a bacterial phytochrome. Science 324, 804–807.

Smith, A.M., Michael, C., and Nie, S. (2009). Bioimaging: second window for in vivo imaging. Nat. Nanotechnol. 4, 710–711.

Song, D., Chi, S., Li, X., Wang, C., Li, Z., and Liu, Z. (2019). Upconversion system with quantum dots as sensitizer: improved photoluminescence and PDT efficiency. ACS Appl. Mater. Interfaces 11, 41100–41108.

Tan, M., Del Rosal, B., Zhang, Y., Martín Rodríguez, E., Hu, J., Zhou, Z., Fan, R., Ortgies, D.H., Fernández, N., Chaves-Coira, I., et al. (2018). Rare-earth-doped fluoride nanoparticles with engineered long luminescence lifetime for time-gated in vivo optical imaging in the second biological window. Nanoscale 10, 17771–17780.

Tang, L., Ji, R., Li, X., Bai, G., Ping Liu, C., Hao, J., Lin, J., Jiang, H., Teng, K.S., Yang, Z., et al. (2014). Deep ultraviolet to near-infrared emission and photoresponse in layered N-doped graphene quantum dots. ACS Nano 8, 6312–6320.

Tang, Z., Zhang, Q., Cao, Y., Li, Y., and Wang, Y. (2020). Eu2+-Doped ultra-broadband VIS-NIR emitting phosphor. Chem. Eng. J. 388, 124231.

Telford, W.G., Shcherbakova, D.M., Buschke, D., Hawley, T.S., and Verkhusha, V.V. (2015). Multiparametric flow cytometry using near-infrared fluorescent proteins engineered from bacterial phytochromes. PLoS One 10, e0122342.

Vogler, A., and Kunkely, H. (2006). Excited state properties of lanthanide complexes: beyond ff states. Inorg. Chim. Acta 359, 4130–4138.

Wang, S., Fan, Y., Li, D., Sun, C., Lei, Z., Lu, L., Wang, T., and Zhang, F. (2019). Anti-quenching NIR-II molecular fluorophores for in vivo high-contrast imaging and pH sensing. Nat. Commun. 10, 1058.

Wei, Y.-C., Fu Wang, S., Hu, Y., Liao, L.-S., Chen, D.-G., Chang, K.-H., Wang, C.-W., Liu, S.H., Hung, W.Y., Wang, T.H., et al. (2020). Overcoming the energy gap law in near-infrared OLEDs by exciton–vibration decoupling. Nat. Photon. 14, 570–577.

Weidman, M.C., Beck, M.E., Hoffman, R.S., Prins, F., and Tisdale, W.A. (2014). Monodisperse,

air-stable PbS nanocrystals via precursor stoichiometry control. ACS Nano 8, 6363–6371.

Weinhard, L., Di Bartolomei, G., Bolasco, G., Machado, P., Schieber, N.L., Neniskyte, U., Exiga, M., Vadisiute, A., Raggioli, A., Schertel, A., et al. (2018). Microglia remodel synapses by presynaptic trogocytosis and spine head filopodia induction. Nat. Commun. 9, 1228.

Welsher, K., Liu, Z., Sherlock, S.P., Robinson, J.T., Chen, Z., Daranciang, D., and Dai, H. (2009). A route to brightly fluorescent carbon nanotubes for near-infrared imaging in mice. Nat. Nanotechnol. 4, 773–780.

Wu, S., Han, G., Milliron, D.J., Aloni, S., Altoe, V., Talapin, D.V., Cohen, B.E., and Schuck, P.J. (2009). Non-blinking and photostable upconverted luminescence from single lanthanide-doped nanocrystals. Proc. Natl. Acad. Sci. U S A 106, 10917–10921.

Wu, J.-J., Gao, H., Lai, R., Zhuo, M.-P., Feng, J., Wang, X.-D., Wu, Y., Liao, L.-S., and Jiang, Lei (2020). Near-infrared organic single-crystal nanolaser arrays activated by excited-state intramolecular proton transfer. Matter 2, 1233–1243.

Xie, X., Li, Z., Zhang, Y., Guo, S., Iris Pendharkar, A., Lu, M., Huang, L., Huang, W., and Han, G. (2017). Emerging ≈800 Nm excited lanthanide-doped upconversion nanoparticles. Small 13, https://doi.org/10.1002/smll.201602843.

Xu, S., Wang, F., Zhu, C., Meng, Y., Liu, Y., Liu, W., Tang, J., Liu, K., Hu, G., Howe, R.C., et al. (2016a). Ultrafast nonlinear photoresponse of single-wall carbon nanotubes: a broadband degenerate investigation. Nanoscale 8, 9304–9309.

Xu, S., Cui, J., and Wang, L. (2016b). Recent developments of low-toxicity NIR II quantum dots for sensing and bioimaging. Trends Anal. Chem. TRAC 80, 149–155.

Xu, X., Shao, Q., Yao, L., Dong, Y., and Jiang, J. (2020). Highly efficient and thermally stable Cr3+-activated silicate phosphors for broadband near-infrared LED applications. Chem. Eng. J. 383, 123108.

Yamashita, S. (2019). Nonlinear optics in carbon nanotube, graphene, and related 2D materials. APL Photonics 4, 034301.

Yu, D., Gustafson, W.C., Han, C., Lafaye, C., Noirclerc-Savoye, M., Ge, W.P., Thayer, D.A., Huang, H., Kornberg, T.B., Royant, A., et al. (2014). An improved monomeric infrared fluorescent protein for neuronal and tumour brain imaging. Nat. Commun. 5, 3626.

Yang, Q., Hu, Z., Zhu, S., Ma, R., Ma, H., Ma, Z., Wan, H., Zhu, T., Jiang, Z., Liu, W., et al. (2018). Donor engineering for NIR-II molecular fluorophores with enhanced fluorescent performance. J. Am. Chem. Soc. 140, 1715–1724.

Yang, Q., Ma, Z., Wang, H., Zhou, B., Zhu, S., Zhong, Y., Wang, J., Wan, H., Antaris, A., Ma, R., et al. (2017). Rational design of molecular fluorophores for biological imaging in the NIR-II window. Adv. Mater. 29, 1605497.

Yu, D., Baird, M.A., Allen, J.R., Howe, E.S., Klassen, M.P., Reade, A., Makhijani, K., Song, Y., Liu, S., Murthy, Z., et al. (2015). A naturally monomeric infrared fluorescent protein for protein labeling in vivo. Nat. Methods 12, 763–765.

Yuan, G., Gómez, D.E., Kirkwood, N., Boldt, K., and Mulvaney, P. (2018). Two mechanisms determine quantum dot blinking. ACS Nano 12, 3397–3405.

Zamberlan, F., Turyanska, L., Patanè, A., Liu, Z., Williams, H.E.L., Fay, M.W., Clarke, P.A., Imamura, Y., Jin, T., Bradshaw, T.D., et al. (2018). Stable DHLA–PEG capped PbS quantum dots: from synthesis to near-infrared biomedical imaging. Journal of materials chemistry. J. Mater. Chem. B 6, 550–555.

Zampetti, A., Minotto, A., and Cacialli, F. (2019). Near-infrared (NIR) organic light-emitting diodes (OLEDs): challenges and opportunities. Adv. Funct. Mater. 29, 1807623.

Zeng, X., Xiao, Y., Lin, J., Li, S., Zhou, H., Nong, J., Xu, G., Wang, H., Xu, F., Wu, J., et al. (2018). Near-infrared II dye-protein complex for biomedical imaging and imaging-guided photothermal therapy. Adv. Healthc. Mater. 7, e1800589.

Zhang, W., Chen, T., Su, L., Ge, X., Chen, X., Song, J., and Yang, H. (2020a). Quantum dot-based sensitization system for boosted photon absorption and enhanced second near-infrared luminescence of lanthanide-doped nanoparticle. Anal. Chem. 92, 6094–6102.

Zhang, Y., Li, Q., Cai, M., Xue, J., and Qiao, J. (2020b). An 850 Nm pure near-infrared emitting Iridium complex for solution-processed organic light-emitting diodes. J. Mater. Chem. 8, 8484–8492.

Zhang, M., Yue, J., Cui, R., Ma, Z., Wan, H., Wang, F., Zhu, S., Zhou, Y., Kuang, Y., Zhong, Y., et al. (2018). Bright quantum dots emitting at ~1,600 Nm in the NIR-IIb window for deep tissue fluorescence imaging. Proc. Natl. Acad. Sci. U S A. https://doi.org/10.1073/pnas.1806153115.

Zheng, D., Fang, H., Long, M., Wu, F., Wang, P., Gong, F., Wu, X., Ho, J.C., Liao, L., and Hu, W. (2018). High-performance near-infrared photodetectors based on P-type SnX (X = S, Se) nanowires grown via chemical vapor deposition. ACS Nano 12, 7239–7245.

Zhu, S., Yang, Q., Antaris, A.L., Yue, J., Ma, Z., Wang, H., Huang, W., Wan, H., Wang, J., Diao, S., et al. (2017). Molecular imaging of biological systems with a clickable dye in the broad 800- to 1,700-nm near-infrared window. Proc. Natl. Acad. Sci. U S A. https://doi.org/10.1073/pnas.1617990114.

Zou, W., Visser, C., Maduro, J.A., Pshenichnikov, M.S., and Hummelen, J.C. (2012). Broadband dye-sensitized upconversion of near-infrared light. Nat. Photon. https://doi.org/10.1038/nphoton.2012.158.